Multi-temporal Canopy Height Modeling using Deep Learning and Sentinel-2: The Influence of Training Data and Input Feature Representations

Felix Wengler[1], David Klehr[1], Alexander Wagner[2], David Frantz[1,*]

Affiliations

[1] Geoinformatics – Spatial Data Science, Trier University, Universitätsring 15, 54296 Trier, Germany
[2] Forschungsanstalt für Waldökologie und Forstwirtschaft Rheinland-Pfalz, Hauptstraße 16, 67705 Trippstadt, Germany

ORCiD/E-Mail

F. Wengler: 0009-0006-0009-7609 wengler@uni-trier.de
D. Klehr: 0009-0006-5461-1677 klehr@uni-trier.de
A. Wagner: 0000-0001-7603-1899 alexander.wagner@wald-rlp.de
D. Frantz*: 0000-0002-9292-3931 david.frantz@uni-trier.de

*Corresponding author

This is a non-peer-reviewed preprint submitted to EarthArXiv. This manuscript will be submitted for publication in a peer-reviewed journal. Subsequent versions of this manuscript may have slightly different content. If accepted, the final version of this manuscript will be available via the 'Peer-reviewed Publication DOI' link on the right-hand side of this webpage.

Abstract

Precise information on canopy height is crucial to assess biomass and climate-induced structural changes within forests. Canopy height maps derived from optical satellite data can provide valuable wall-to-wall information, but often remain subject to substantial uncertainties. In this study, we systematically investigate the influence of training data and Sentinel-2 feature representations on the statistical performance of multi-temporal, deep learning-based canopy height modeling within Rhineland-Palatinate, Germany. We trained separate models using GEDI canopy height metrics or photogrammetric digital surface models (pDSM) as training data, and compared Sentinel-2 composites with spline coefficients derived from annual satellite time series as input representations. Hence, four different canopy height models were generated for the period 2018–2025, which we validated with independent airborne LiDAR data and compared with established global canopy height products. The best predictions were achieved using a combination of pDSM training data and Sentinel-2 spline coefficients, reaching a pooled RMSE of 3.14 m, compared to 4.06 m - 5.98 m for the other model configurations. This improvement was mainly rooted in the higher inherent accuracy of pDSM data, as well as the phenological information provided by the spline coefficients. The best-performing model also outperformed three global canopy height products and exhibited high temporal stability, supporting its suitability for a range of forest monitoring applications such as disturbance and recovery monitoring.

Keywords: canopy height modeling; deep learning; Sentinel-2; Sentinel-1; GEDI; digital surface model; airborne laser scanning; spline coefficients

1 Introduction

Forests account for approximately 80% of global terrestrial biomass and therefore play a crucial role in the global carbon cycle and the mitigation of climate change through carbon sequestration (Nunes et al., 2020; Pan et al., 2013). Over the past decades, European forests have been subject to severe alterations, mostly due to increasing disturbances driven by ongoing climate change (Grünig et al., 2026; Senf & Seidl, 2021). In this context, information on forest structure, such as canopy height, is becoming increasingly relevant, as it serves as an important determinant of biomass and is well-suited for the monitoring of disturbances and recovery (F. Fassnacht et al., 2014; Lang et al., 2023; Senf et al., 2019). Remote sensing can provide precise information on canopy height at high spatial resolution through the utilization of Airborne Laser Scanning (ALS) or photogrammetric correlation of aerial imagery (Coops et al., 2021; Haala, 2011). Their acquisition, however, is costly, often resulting in sparse and fragmented spatial coverage as well as temporal inconsistencies, including data being acquired years apart or under differing conditions (e.g., leaf-on vs. leaf-off periods) (Moudrỳ et al., 2026). This complicates their consistent use for multi-temporal applications.
To overcome this limitation, recent research has focused on the utilization of high-, to medium-resolution, openly available satellite imagery, such as Sentinel-2, Sentinel-1 and Landsat, in combination with sparse LiDAR reference data for modeling and predicting canopy height with wall-to-wall coverage. The most widely used source of reference data is the Global Ecosystem Dynamics Investigation (GEDI), a spaceborne LiDAR mission providing forest structure information within non-contiguous 25 m diameter footprints, spaced approximately 600 m across-track and 60 m along-track (Dubayah et al., 2020). It has shown to be well suited for integration with satellite imagery in machine learning frameworks to generate spatially continuous canopy height maps (Kacic et al., 2023; Potapov et al., 2021; Turubanova et al., 2023). In recent years, deep learning architectures have been shown to generate more accurate maps of canopy height at global (Lang et al., 2023; Pauls et al., 2026), continental (De Keersmaecker et al., 2026) and national (Schwartz et al., 2023) scale.

However, the accuracy of these maps remains limited, as the GEDI footprints themselves can be affected by substantial errors, primarily due to geolocation inaccuracies, terrain slope, and beam type (Adam et al., 2020; Tang et al., 2023). Furthermore, GEDI-footprints over very short or absent canopies are subject to a systematic bias of approximately 3 m (Pauls et al., 2024), which makes utilization for young forest stands challenging. A known issue of canopy height maps using GEDI reference data also remains the underprediction of tall canopies and the overestimation of small canopies (Chen et al., 2025; Dong et al., 2025; Moudrỳ et al., 2024a). This limits their applicability for tasks such as early forest recovery monitoring. Due to their higher accuracy and lower sensitivity to geolocation and terrain-related errors, digital surface models derived from ALS (aDSM) and photogrammetric imagery (pDSM) have the potential to mitigate or at least reduce these limitations when used as reference data for wall-to-wall canopy height modeling (Moudrỳ et al., 2026). Although several studies have successfully used ALS data for this task (Kalinicheva et al., 2026; S. Liu et al., 2023), to our knowledge, a systematic comparison between GEDI and airborne-derived DSMs as training reference data for canopy height modeling has not yet been conducted. While ALS offers the highest accuracy among these reference sources (Nurminen et al., 2013), its availability relative to pDSMs varies regionally, as photogrammetric image acquisition is generally more cost-effective and efficient, as it is often carried out routinely by surveying agencies.

Besides the choice of reference data, the representation of the satellite imagery itself may also influence the accuracy of canopy height modeling. Many existing canopy height products rely on annual or seasonal satellite image composites as input features, as they provide cloud-free observations while reducing atmospheric effects and data volume (Griffiths et al., 2013). However, such selection approaches compress an entire

time series into a single synthetic image and therefore discard the valuable temporal information contained within the original satellite time series. To retain more of this temporal information, spectral-temporal metrics (STMs) have been used for canopy height modeling (Potapov et al., 2021; Turubanova et al., 2023). STMs aggregate satellite imagery time series into a set of statistical metrics, thereby retaining beneficial temporal information (Frantz et al., 2023a). Recent studies have demonstrated that utilizing satellite image time series directly improves canopy height modeling performance, e.g., Kalinicheva et al. (2026). Similarly, Earth observation foundation models exploit complete satellite time series to derive temporal embeddings that have shown promising results for canopy height prediction (Feng et al., 2026). Alternative temporal representations can be derived from the statistical coefficients of time series interpolation. Similar to embeddings, these produce a continuous, gap-free signal, preserving seasonal surface dynamics such as vegetation phenology and serve as a compact, dimensionality-reduced representation of the time series. Such a feature space has been shown to improve predictive performance for modeling forest inventory metrics compared to image composites (Wilson et al., 2018). Recently, spline coefficients derived from cubic spline interpolation of the time series (Bolton et al., 2020) have been successfully applied to derive forest information layers, e.g., tree species fractions (Klehr et al., 2025), and have shown to outperform STMs, and perform on par with latent embeddings for land cover fraction mapping (Schug et al., 2026). However, their suitability for canopy height modeling remains unexplored.

Consequently, the aim of this study is to systematically investigate two key factors that may affect the accuracy of deep learning-based canopy height modeling: 1) the choice of training reference data and 2) the temporal representation of the satellite input data, which, to our knowledge, have not yet been jointly assessed. Four deep learning models are trained, covering all combinations of two training data sources (GEDI footprints and pDSMs) and two Sentinel-2 input representations (median composites and spline coefficients), to assess their individual and combined effects on the accuracy of canopy height modeling in a temperate mixed forest region. Sentinel-1 SAR data are additionally included as a standard complementary input across all model configurations. The resulting multi-temporal canopy height maps are evaluated using independent ALS-derived reference data.

2 Study Area

Our study area comprises the federal state of Rhineland-Palatinate in southwestern Germany (Figure 1). Approximately 43% of the state's land area is covered by forests, making it the most densely forested federal state in Germany. Forests are dominated by European beech, oak, and Norway spruce. The severe drought events between 2018 and 2020 resulted in extensive bark beetle outbreaks and widespread mortality of spruce stands, particularly in the northern parts of the state (Landesforsten Rheinland-Pfalz, 2022). This led to diverse forest conditions, ranging from mature, closed stands to recently disturbed and regenerating areas including standing deadwood in non-managed national park areas. Together with multi-temporal availability of both pDSM and aDSM data, this makes Rhineland-Palatinate a suitable area for the evaluation of canopy height modeling.
The region is furthermore characterized by a temperate oceanic climate and a heterogeneous topography that strongly influences local climatic conditions and forest structure (Gauer, 2012).

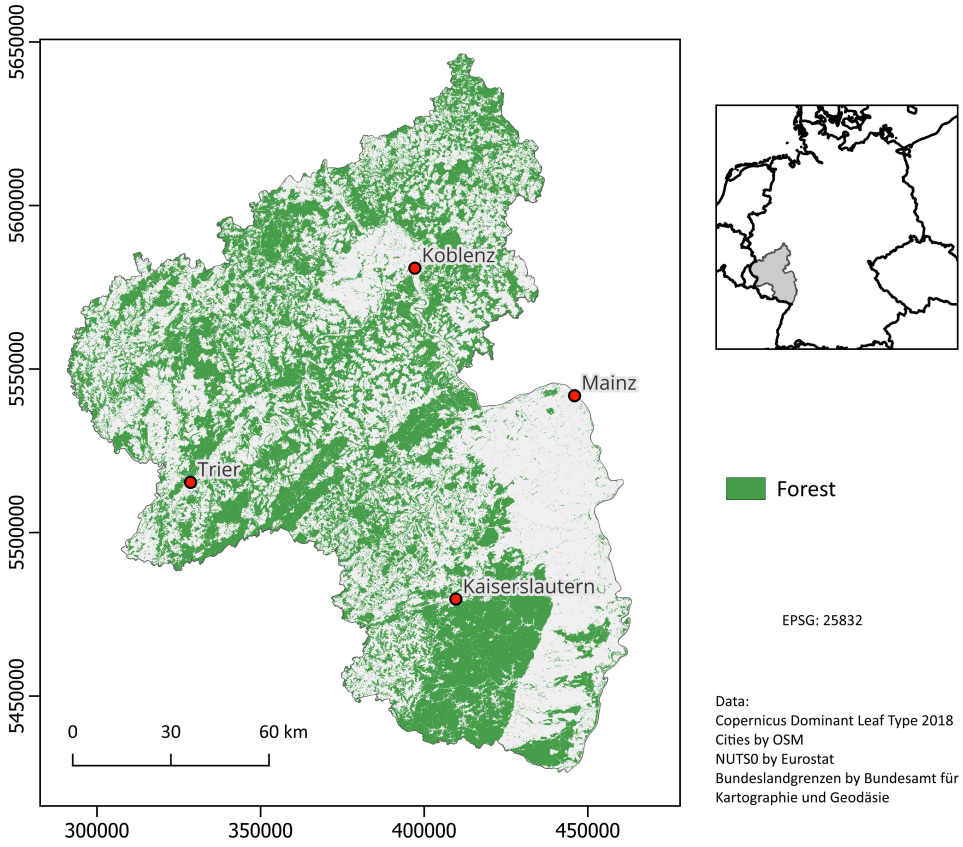


Figure 1: Overview of the study area: Rhineland-Palatinate, federal state of Germany.

3 Data

3.1 Satellite Data

All available Sentinel-2 Level 1C images covering Rhineland-Palatinate were acquired for the period 2018–2025. It yields multispectral Earth observation data with a band-specific spatial resolution between 10 and 60 m. Three satellites (A, B, and C) provide revisit frequencies of around 2–3 days at mid-latitudes (Drusch et al., 2012). To ensure standardized and efficient downstream analysis, the data were processed into Analysis Ready Data (ARD) and stored in a data cube structure using the Framework for Operational Radiometric Correction for Environmental Monitoring (FORCE) (Frantz, 2019). Preprocessing comprised cloud masking, as well as radiometric, atmospheric, topographic and bi-directional reflectance distribution function corrections (Buchner et al., 2020; Frantz et al., 2016a, 2018; Roy et al., 2017). Furthermore, the spatial resolution of the 20 m bands was improved to 10 m resolution using the ImproPhe data fusion algorithm (Frantz et al., 2016b).

Additionally, Sentinel-1 gamma naught (γ^0) data were acquired for the same research period through the CODE-DE platform (https://code-de.org/de/portfolio/?q=Sentinel-1). Sentinel-1 acquires C-band Synthetic Aperture Radar (SAR) data using multiple sun-synchronous satellites with a revisit time of 1 to 3 days (Torres et al., 2012). Preprocessing included radiometric calibration, multilooking, as well as topographic and geometric corrections. Ground Range Detected (GRD) observations were acquired in both VV and VH polarizations and were also organized in a data cube format (Beyer et al., 2025).

3.2 Canopy Height Reference Data

3.2.1 GEDI

Two different data sources were acquired for the training of the employed deep learning models. The Global Ecosystem Dynamics Investigation (GEDI) data provides global forest structure measurements within circular footprints of approximately 25 m in diameter (Dubayah et al., 2020). In this study, the RH95 metric, representing the height below which 95% of the waveform energy is returned relative to the ground, was used as the canopy height reference, as it has been shown to correlate well with canopy height while being less sensitive to noise (Schwartz et al., 2024). All available GEDI footprints covering Rhineland-Palatinate were acquired for the years 2019–2022 and 2024; the instrument went into a hibernation phase in 2023. To ensure high-quality training labels the GEDI data were filtered using quality and degrade flags, a sensitivity threshold greater than 0.95, and the selection of power beams only. After filtering, a total of 579,168 GEDI footprints were retained for training.

3.2.2 Photogrammetric Digital Surface Model

The second source of training data consists of photogrammetric digital surface models (pDSMs). These models are generated from dense point clouds derived through the photogrammetric correlation of overlapping aerial images, resulting in wall-to-wall surface information (Haala, 2011). They cover approximately half of the study area each year, provide a vertical accuracy of approximately 1 m, and were provided by the State Office for Surveying and Geobasis Information of Rhineland-Palatinate (LVermGeoRLP, 2026). For this study, pDSMs were available for the years 2018, 2019, 2020, 2022, and 2023 at a spatial resolution of 20 cm, with acquisition dates mostly between June and August (Figure A1). The pDSMs were resampled using maximum resampling to 5 m and bilinear resampling to 10 m. They were visually inspected, to ensure high-quality training data. Regions with obvious data artifacts were manually removed. As pDSMs are acquired in regular cycles with high spatial coverage in Germany, their availability for large-scale rollout is much better than that of ALS data. Hence, they were used as training data in this study.

3.3 ALS-based Digital Surface Model

To independently validate the canopy height models, ALS-derived digital surface models (aDSMs) acquired between 2020 and 2025 were used. The ALS acquisitions were carried out as part of a multi-year surveying campaign during leaf-off conditions, with the datasets from 2020 to 2024 collectively covering the entire study area, while the 2025 acquisition provides additional coverage (Figure A2). The data were provided by the State Office for Surveying and Geobasis Information and have a reported vertical accuracy better than 30 cm. Owing to their high accuracy, the aDSMs were used exclusively for independent model validation – in line with good practice guidelines stating that validation data shall be of better quality than the data used for training (Olofsson et al., 2014). They were resampled and visually inspected, consistent with the pDSMs.

3.3.1 Additional Data

Daily surface temperature data, specifically soil temperature at 5 cm depth, were obtained from the Climate Data Center of the German Meteorological Service (DWD – German Meteorological Service, 2026). The dataset provides spatially continuous daily estimates at a spatial resolution of 1 km, derived using the agrometeorological soil-plant-atmosphere model AMBETI (Braden, 1995) and subsequent spatial interpolation. The data were reprojected to ETRS89-LAEA (EPSG:3035) to align with the Sentinel-2 data and

provide the basis for thermal encoding of the Sentinel-2 time series, which is part of the workflow to derive the spline coefficients.

To compare our canopy height model configurations with established products, three global canopy height maps for the year 2020 were used as a benchmark. These comprised ECHOSAT by Pauls et al. (2026), the Very High Resolution Canopy Height Maps by Tolan et al. (2024), and the Canopy Height Model of the Earth by Lang et al. (2023).

Additionally, the Copernicus Dominant Leaf Type layer for 2018 was used to constrain height predictions to forested areas during validation (Copernicus Land Monitoring Service, 2020). During the spatiotemporal analysis, the Forest Canopy Cover Loss dataset for Germany (Thonfeld et al., 2026) was used to differentiate disturbed areas from unaffected areas. To identify standing deadwood for the temporal analysis of disturbed areas, the standing deadwood fractions for Germany by Schiefer et al. (2025) were used.

4 Methodology

This section outlines the methodological approach of this study, which compares four different model configurations combining different training reference data sources (GEDI and pDSM) and Sentinel-2 input representations (median composites and spline coefficients), and evaluates their performance against independent ALS data (Figure 2).

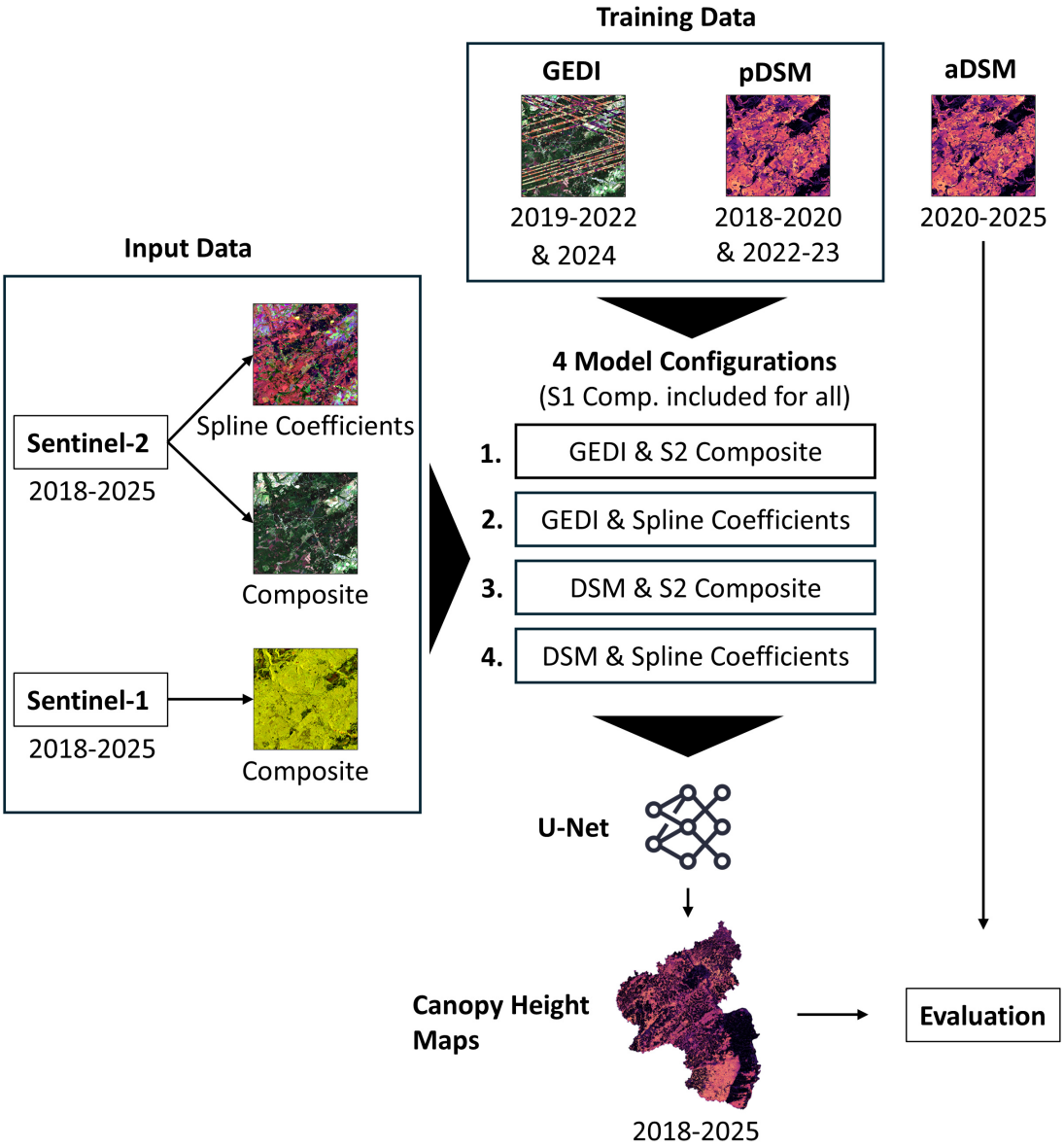


Figure 2: General workflow for this study. Sentinel-1 VV and VH data are used as median composites in all 4 modeling configurations, which consisted of GEDI labels and Sentinel-2 composites (1.), GEDI labels and Sentinel-2 spline coefficients (2.), pDSM labels and Sentinel-2 composites (3.), and pDSM labels and Sentinel-2 spline coefficients (4.). Individual models were trained for the prediction of 4 canopy height time series (2018-2025) for the study area, which were evaluated against independent aDSM reference data.

4.1 Data Preparation

4.1.1 Satellite Composites

For the first and third experimental configurations (Figure 2), Sentinel-2 imagery was aggregated into annual median composites. This represents an established approach, which has been successfully applied for canopy height modeling at various scales, as it reduces noise and residual cloud artifacts while producing representative features of the underlying time series (Pauls et al., 2024; Schwartz et al., 2024). Sentinel-2 images were filtered for clouds and cloud-shadows and composited for the period June to August, matching the acquisition window of most orthophotos used for the pDSMs, to ensure temporal consistency between the satellite input and the training reference data (Figure A1). Sentinel-1 composites were created for VV and VH polarizations in the same manner and used across all model configurations.

4.1.2 Sentinel-2 Time-Series Representation

To represent the temporal dynamics contained within the Sentinel-2 observations, we transformed the irregular image time series into a continuous representation using weighted cubic B-splines, following the original approach of (Bolton et al., 2020). This approach incorporates observations from adjacent years while retaining the temporal characteristics of the target year. The concept of spline fitting has previously been adapted to various remote sensing tasks (Klehr et al., 2025; Schug et al., 2026). We adopted the general framework while modifying the weighting strategy, spline parameterization and implementing a thermal positional encoding, which are described below.

To account for spatial variations in phenological development, we incorporated thermal positional encoding (TPE) following the Nyborg et al. (2022) framework. It represents the temporal position of each Sentinel-2 observation based on accumulated thermal time instead of calendar time. We calculated growing degree days from daily soil temperature data provided by the German Meteorological Service (DWD – German Meteorological Service, 2026), accumulating temperatures above 0 °C and limiting daily contributions to a maximum of 30 °C. The resulting thermal time per day and pixel within a 1km grid, defined by the input data, was normalized to the annual 365-day range to provide a consistent temporal representation across the study area.

For each target year, thermally encoded Sentinel-2 observations from the target year and the two preceding years were considered. Observations from the target year were assigned a base weight of 1.0, whereas observations from the preceding and the second preceding year were assigned initial maximum base weights of 0.30 and 0.15, respectively. Thus, observations from previous years complemented the reconstruction in cases where observations from the target year were sparse, while retaining a substantially lower influence on the resulting temporal representation if data density in the target year was sufficient.

The initial weights were further refined using a residual-based weighting scheme: an initial cubic B-spline was fitted to an NDVI time series constructed from the available observations for each year. The relative residuals between observed and fitted NDVI values were used to down-weight observations with large deviations from the fitted temporal pattern. This residual-based weighting reduces the impact of outliers and observations that are inconsistent with the dominant phenological signal. The resulting weights were then used for the final spline fitting of the Sentinel-2 spectral bands.

For each spectral band, we fitted a smoothed cubic B-spline using 22 basis functions (control points) and uniformly spaced, fixed knots throughout the year. A fixed regularization parameter ($\lambda = 0.1$) controlled the smoothness of the fitted functions by penalizing excessive curvature. The regularization term was based on the integrated squared second derivative of the fitted B-spline, such that functions with greater curvature received a higher penalty. To reduce boundary effects, the annual time series was extended by three observations at both the beginning and end of the year. These additional observations were generated from median values of observations near the respective temporal boundaries.

The resulting 22 spline coefficients per spectral band - derived from thermally encoded observations - were retained as the thermal/temporal features for subsequent analysis. The time-series parameter calculation was implemented in C, and the source code is publicly available at https://github.com/ForestPulse/splinecoefs.

4.1.3 Data Partitioning

For model training, the satellite image representations as well as the reference training data were reshaped into chips of 256×256 pixels; chip dimensions of 2^x have been shown to be efficient for tensor calculations (Cira et al., 2024). GEDI labels were rasterized onto a 10 m grid aligned with the satellite imagery and chipped accordingly. Each RH95 footprint was assigned to the pixel corresponding to the footprint's center. Empty chips, i.e., without any GEDI-labels, were discarded. As GEDI's 25 m footprint diameter exceeds the 10 m pixel resolution, this single-pixel assignment provides a conservative label without assuming ho-

mogeneity within the footprint, though it also inherits uncertainty from GEDI's geolocation error. This approach has been shown to yield stable results for canopy height modeling (Schwartz et al., 2024). Unlike the sparse GEDI-derived chips, which only contain valid pixels at footprints, pDSM-derived chips provide dense, wall-to-wall reference values across the full chip.

The data were split into 80% training and 20% validation data using spatially coherent validation areas distributed across the study area, to avoid overoptimistic accuracy estimates caused by spatial overfitting (Meyer et al., 2018) (Figure 3). To further reduce this effect, the split was applied consistently across all years, and chips located at the border of validation areas were removed. Furthermore, as GEDI and pDSM reference data were not available for every year in the study period (Table A1), each configuration is characterized by years for which no training data were used at any location (temporal holdout years), but independent aDSM validation data were nonetheless available. These years (2023 and 2025 for the GEDI-based configurations; 2024 and 2025 for the pDSM-based configurations) allow for an assessment of temporal stability for years entirely unseen during training. In total, 4,032 training and 1,018 validation chips across all years were used for the pDSM-based modeling and 4,739 training and 1,090 validation chips across all years were used for the GEDI-based modeling. The temporal distribution of training and validation chips is relatively balanced across years for both reference data sources (Table A1), while their spatial distribution differs: pDSM chip density is lower in the north-west of the study area, and GEDI chip density is concentrated along the orbital tracks (Figure 3).

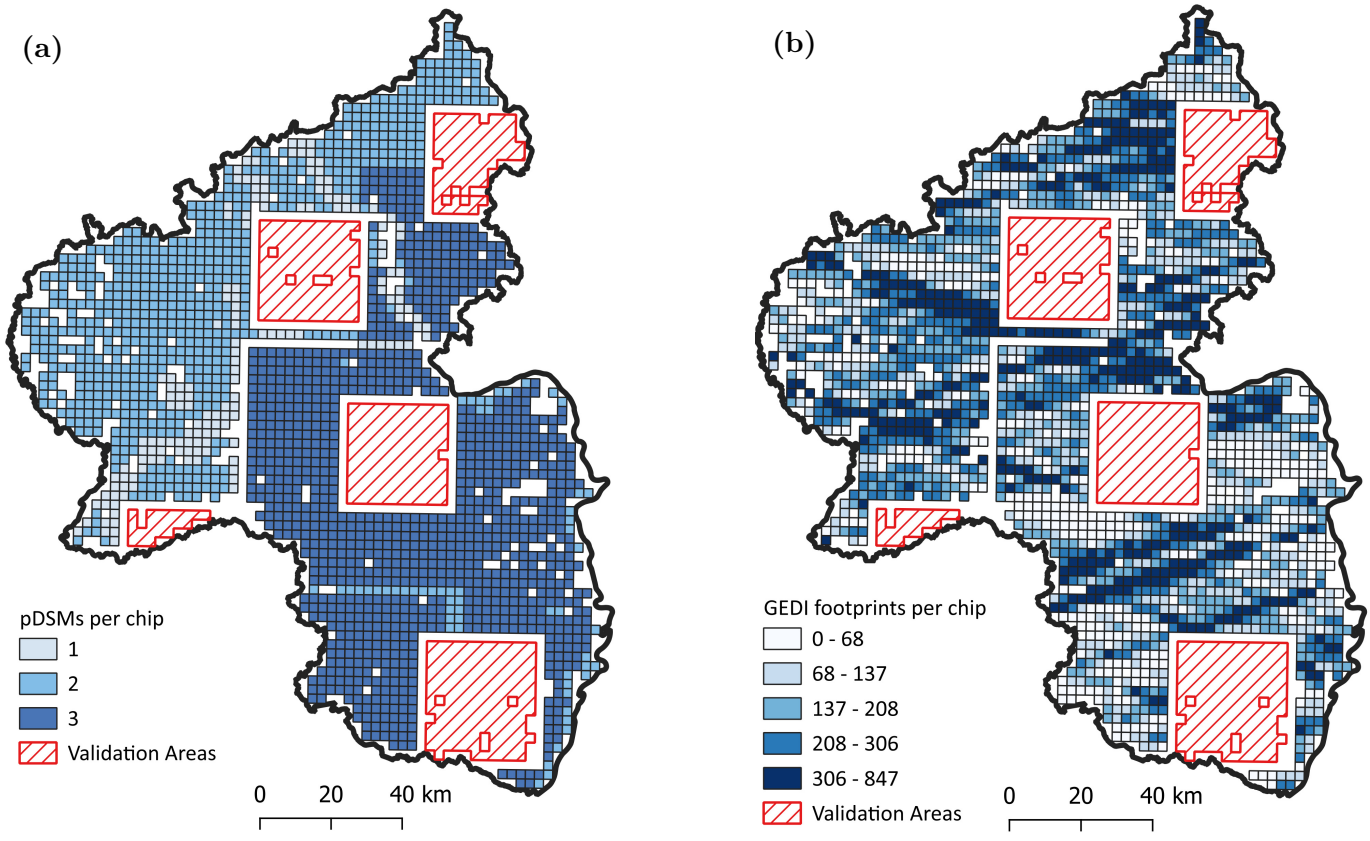


Figure 3: Distribution of reference data availability per chip for multi-temporal photogrammetric DSMs (a) and multi-temporal GEDI footprints (b). The sum of all years is displayed. Held-out validation areas are highlighted. Missing chips were removed because of label noise or to mitigate spatial autocorrelation around validation regions.

4.2 Deep Learning Model

The model used in this study is based on a U-Net architecture, extended with several modifications (Ronneberger et al., 2015). First, Sentinel-1 and Sentinel-2 imagery are processed through separate convolutional stems and fused via concatenation at full spatial resolution (256×256 pixels), prior to entering the encoder. This early-fusion design allows SAR and optical information to be jointly considered from the first encoder level onward. Second, each encoder level consists of two parallel residual blocks with differing kernel sizes (3×3 and 7×7). While the residual blocks allow for deeper and more stable training, the parallel kernels capture both fine-scale and broader spatial context (He et al., 2016; R. Li et al., 2022). Each residual block employs Group Normalization and includes a residual connection with a 1×1 convolution to match channel dimensions where necessary (Wu & He, 2018). Third, skip connections between encoder and decoder include attention gates, which suppress irrelevant spatial regions in the encoder features (Oktay et al., 2018). The encoder comprises three downsampling levels (via max pooling) followed by a bottleneck layer, and the decoder mirrors this structure using transposed convolutions for upsampling. A final 1×1 convolution maps the decoder output to a single-channel canopy height prediction. The only architectural difference between the Sentinel-2 composite- and spline-coefficient-based models lies in the number of input channels of the Sentinel-2 stem (10 and 220 channels, respectively), reflecting the different dimensionality of the two input representations. All other components remain identical across configurations.

Weighted loss functions have shown the potential to mitigate the known tendency of canopy height models to over- and underestimate short and tall canopies (Fayad et al., 2024). Consequently, a weighted loss function was implemented based on an L1 loss. Canopy heights were discretized into eight bins (0–5, 5–10, 10–15, 15–22, 22–30, 30–35, 35–40 and 40–60 m), which were chosen empirically from the error distribution of an initial, unweighted baseline model. Each bin was assigned a weight derived from its Root Mean Square Error (RMSE) in this baseline model, relative to the mean RMSE across all bins:

$$w_k \propto \mathrm{RMSE}_k / \overline{\mathrm{RMSE}} \tag{1}$$

where RMSE_k denotes the RMSE of bin k and $\overline{\mathrm{RMSE}}$ the mean RMSE across all bins. Bins with above-average error were assigned proportionally higher weights, penalizing errors within these bins more strongly during training. The resulting weights were normalized to a mean of 1 and clamped to a fixed range to preserve training stability. During training, the loss for each pixel was computed as the absolute error between prediction and reference, scaled by the weight of the bin corresponding to the reference height:

$$\mathcal{L} = \frac{1}{N} \sum_{i=1}^{N} w_{k(i)} \, |\hat{y}_i - y_i| \tag{2}$$

where N is the number of valid pixels in a chip and $k(i)$ is the bin index corresponding to the reference height of pixel i.

4.3 Experimental Design

The training process was kept largely identical for all four experimental configurations. Matching Sentinel-2, Sentinel-1, and reference label chips were sampled with a batch size of 8 and passed through the model architecture. As the number of available training chips differs between reference data sources due to GEDI's sparse, point-based sampling versus the dense, wall-to-wall coverage of the pDSM, the full training split was used for each configuration. This was done to ensure the maximum achievable modeling accuracy attainable from each reference data source for the given data availability in the study area. Model predictions were

compared to the reference data and the weighted loss was computed. Model weights were updated via back-propagation using the Adam optimizer (Kingma & Ba, 2014). The initial learning rate was set to 0.0001 and reduced by a factor of 2 if the validation error metric did not improve for 5 consecutive epochs. After each epoch, the error metric was calculated using the held-out 20% validation data, and the model checkpoint was saved whenever a new lowest value was achieved. For the pDSM-based configurations, the RMSE was used and for the GEDI based configuration the Mean Absolute Error (MAE), as it is less sensitive to outliers, which are more likely in noisy GEDI labels (Hodson, 2022). The same validation areas were used across all configurations to ensure comparability. No data augmentation was applied. Each model was trained for 100 epochs on an NVIDIA GeForce RTX 3050 (6 GB VRAM), with training times ranging from 26–41 hours depending on the configuration. All models were implemented using the Python library PyTorch (Paszke et al., 2019).

Based on this shared structure, four model experiments were conducted: (1) sparse GEDI-labels combined with Sentinel-2 composites, (2) sparse GEDI-labels combined with Sentinel-2 spline coefficients, (3) wall-to-wall pDSM-labels combined with Sentinel-2 composites, and (4) wall-to-wall pDSM-labels combined with Sentinel-2 spline coefficients. This design allows to assess the individual and combined effects of training data and input representations on canopy height modeling (Figure 2). Sentinel-1 composites were used as complementary input data in all training scenarios. For the GEDI-based configurations, only valid pixels were used in the loss computation. From each model experiment, canopy height maps were generated for the years 2018 to 2025 for the complete study area at 10 m spatial resolution.

4.4 Evaluation Metrics

To evaluate and compare the four canopy height models, predictions were validated against independent aDSM reference data, matched by acquisition and prediction year. As the aDSM data were not used during initial training and validation in any of the configurations, they provide a consistent and unbiased basis for comparison across all experiments. Furthermore, only aDSM data within the validation areas were used to ensure spatial independence during accuracy assessment (Figure A2). All evaluations were restricted to forested areas using the 2018 tree mask. Multiple error metrics were computed to assess model accuracy: the Root Mean Squared Error (RMSE), the Mean Absolute Error (MAE), and the coefficient of determination (R^2), representing the proportion of variance in the reference data explained by the model predictions. The metrics are reported annually, as well as pooled across all years in which reference data were available. For the pooled analysis, slope and intercept are reported as well.
To further investigate the influence of reference data and input representation on the prediction of specific canopy heights, such as short and tall canopies, RMSE was additionally computed within 2 m height bins of the pooled validation data and compared between the four configurations. The canopy height map based on pDSM training data and spline coefficients was further compared against three established global canopy height products for the year 2020, using the same set of metrics and the same aDSM-based, masked evaluation approach.

To assess the suitability of the multi-temporal predictions for various downstream applications, a temporal analysis of the best-performing model was conducted. Canopy height change between 2018 and 2025 was evaluated annually, while pixels that were flagged by the Forest Canopy Cover Loss disturbance product were omitted (Thonfeld et al., 2026). This was done to investigate the ecological plausibility of the annual height change between years for several height-bins, without disturbed areas.
Furthermore, we evaluated height changes in areas disturbed between 2019 and 2021. Disturbed pixels were differentiated into standing deadwood and other disturbances using the Germany-wide standing deadwood

probability product of Schiefer et al. (2025). To obtain a conservative standing-deadwood sample, only pixels with a probability of at least 80% were classified as standing deadwood, with all remaining disturbed pixels classified as other disturbances. To reduce mixed-pixel effects along disturbance boundaries, a one-pixel interior buffer was removed from the disturbance mask. For each disturbed pixel, canopy height change was calculated relative to the year preceding the disturbance and trajectories were aligned to the disturbance year. In addition, standing-deadwood trajectories within Hunsrück-Hochwald National Park, where dead trees are generally not subject to salvage logging, were compared with the corresponding trajectories derived from the full study area.

5 Results

5.1 Quantitative Results

The results of the pooled accuracy assessment show substantially different performance depending on the model configurations (Figure 4). The pDSM-Spline model reaches the best overall MAE (2.31 m), RMSE (3.14 m) and R^2 (0.86), while the GEDI-Composite model performs worst (MAE: 4.52 m, RMSE: 5.98 m, R^2: 0.51).

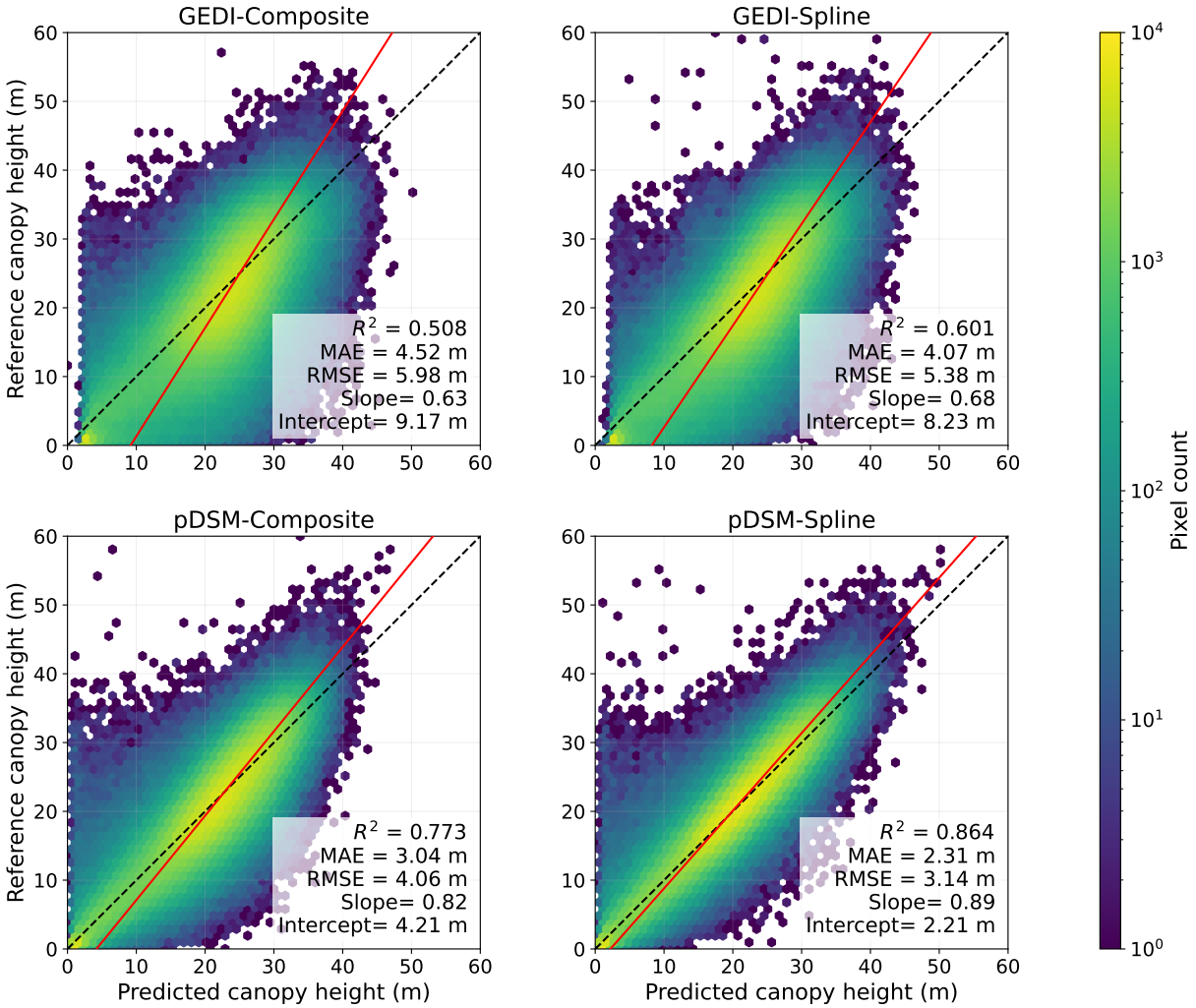


Figure 4: Comparison of predicted against aDSM canopy heights for the four canopy height models using all validation pixels pooled across years. The dashed line indicates the 1:1 relationship and the red line shows the linear regression fit. The color scale indicates the number of observations per hexagonal bin and is shared across all panels.

Comparing models that use the same input representations shows that replacing GEDI with pDSMs improves the accuracy substantially for the composite-based (MAE by 1.48 m, RMSE by 1.92 m and R^2 by 0.265) and the spline-based configurations (MAE by 1.76 m, RMSE by 2.24 m and R^2 by 0.263), with a slightly larger absolute increase for MAE and RMSE when using spline coefficients. Consequently, comparing models with the same training reference data shows the effect of the input data representations. Replacing Sentinel-2 composites with spline coefficients improves all error metrics for the GEDI-based (MAE by 0.45 m, RMSE by 0.60 m and R^2 by 0.093) and the pDSM-based configurations (MAE by 0.73 m, RMSE by 0.92 m and R^2 by 0.091). Overall, pDSM training data have a larger effect on model accuracy, although spline coefficients also show considerable improvements for both training data types. This pattern is also reflected in the regression slope and intercept. The slope increases from 0.63 for GEDI-Composite to 0.89 for pDSM-Spline, while the intercept decreases from 9.17 m to 2.21 m, indicating a reduction in modeling bias.

These improvements also persist for the annual error metrics (Table 1). For every year, the pDSM-Spline model achieves the best scores across all error metrics, followed by pDSM-Composite, GEDI-Spline, and GEDI-Composite. Annual sample sizes range roughly from 940,000 to 5,420,000 pixels, reflecting differences in aDSM validation data availability within the spatial holdout. While RMSE and R^2 are subject to substantial interannual fluctuations for the GEDI-Composite model (SD: RMSE = 0.57 m, R^2 = 0.07) the pDSM-Spline model achieves more stable interannual results (SD: RMSE = 0.34, R^2 = 0.02), suggesting improved robustness for multi-temporal predictions. Notably, temporal holdout years, from which no data were used during training, regardless of location, do not show systematically higher errors than years for which the model had seen data, suggesting that all four models generalize reasonably well for unseen years.

Table 1: Annual accuracy assessment of the four canopy height models. MAE and RMSE are reported in meters. Grey-shaded cells indicate temporal holdout years, i.e., no data from the corresponding year was used to train the respective model. Standard deviation (SD) for each metric is reported in the last row.

Year	**GEDI-Composite**			**GEDI-Spline**			**DSM-Composite**			**DSM-Spline**		
	MAE	**RMSE**	R^2	**MAE**	**RMSE**	R^2	**MAE**	**RMSE**	R^2	**MAE**	**RMSE**	R^2
2020	4.22	5.61	0.49	3.74	4.98	0.60	2.64	3.55	0.80	2.02	2.77	0.88
2022	4.57	6.09	0.36	4.35	5.69	0.44	3.01	3.98	0.73	2.51	3.32	0.81
2023	3.77	4.96	0.47	3.51	4.67	0.53	2.56	3.34	0.76	1.98	2.63	0.85
2024	5.15	6.66	0.46	4.38	5.74	0.60	3.62	4.77	0.72	2.46	3.38	0.86
2025	4.63	6.10	0.59	3.90	5.18	0.71	3.05	4.24	0.80	2.36	3.45	0.86
SD	0.46	0.57	0.07	0.34	0.41	0.09	0.38	0.51	0.03	0.22	0.34	0.02

The binned absolute RMSE shows how uncertainty varies across different canopy heights (Figure 5). Medium canopy heights (22-30 m) already show comparatively low errors for both GEDI models, with only moderate improvement for the pDSM-Composite and pDSM-Spline models. The largest improvement can be observed for short canopy heights (2-12 m), where RMSE improved by approximately 5 to 7 meters between the GEDI-Composite and the pDSM-Spline model (Table A2). Within the GEDI-based configurations, spline coefficients also reduce RMSE consistently, though this improvement is most pronounced at short canopy heights and comparatively small in the medium-height range, where both GEDI models achieve their lowest errors. While all models show increasing error metrics for canopies taller than 30 m, this effect is substantially reduced through the incorporation of the pDSM and spline coefficients.

This pattern is also reflected in the relative binned RMSE (normalized by reference height) Figure 5), which further emphasizes the performance differences for shorter canopies. The pDSM-Spline model reduces the

overall relative RMSE roughly by a factor of 2 compared to the GEDI-Composite model (15.6% vs. 29.6%). As expected, relative RMSE is largest within the smallest height-bin for all configurations, though this error is substantially reduced for the pDSM-Spline configuration (approximately 208%) when compared with the GEDI-Composite configuration (approximately 900%). The relative error decreases for taller bins, before slightly rising again for heights above 30m (Table A3), consistent with the underprediction of tall canopies discussed above. However, this effect is again substantially reduced for the pDSM-Spline model, which achieves the lowest relative RMSE across all bins.

Overall, both the pDSM-Composite and the pDSM-Spline model perform better for every height bin than the GEDI-based models (Table A2). Notably, both the shortest and tallest canopy height bins are represented by comparatively few validation pixels, which has to be considered when interpreting these results.

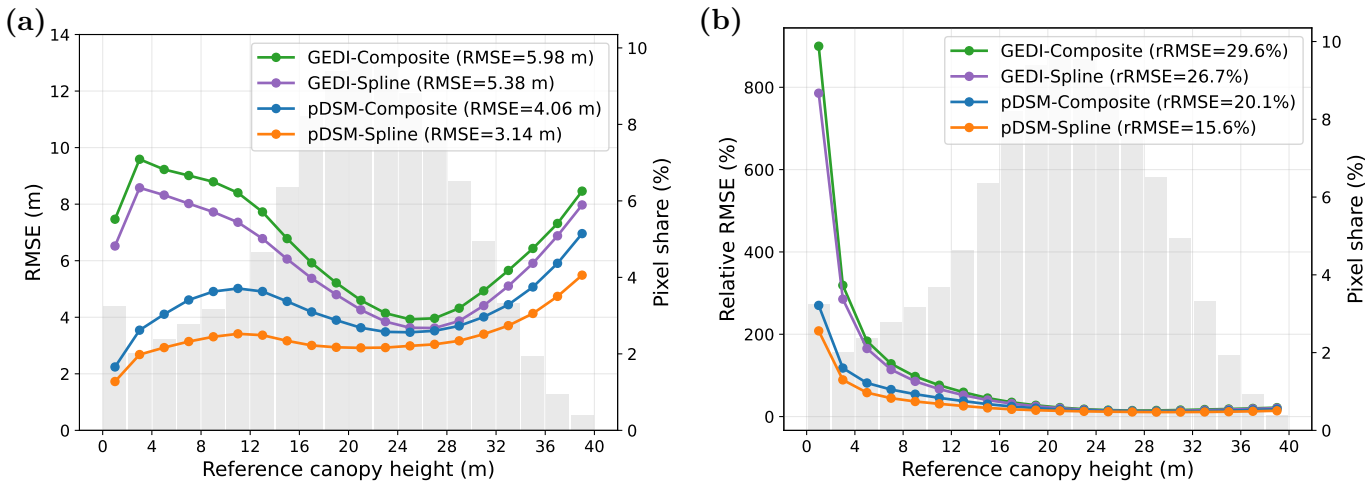


Figure 5: Absolute (a) and relative (b) RMSE distribution within 2 m canopy height bins for the GEDI-Composite, GEDI-Spline, pDSM-Composite, and pDSM-Spline models, pooled over all validation years. Grey bars correspond to the overall proportion of validation pixels within each bin.

5.2 Spatiotemporal Analysis

To visually assess the differences between the model configurations, four representative areas were selected within the spatially held-out validation regions (Figure 6). They were selected to capture a range of forest types and structure within the study area. For each area, the comparison includes the four modeled canopy height configurations, as well as ALS-based ground truth and a corresponding orthophoto (Figure 7).

In areas A and B, the pDSM-based models exhibit substantially more defined forest edges and clearer differentiation between adjacent stands, compared to the GEDI-based models, which in general appear more blurred. This enhanced contrast enables the visibility of small-scale differences in both vertical and horizontal canopy structure. This is particularly evident in area D, where the GEDI-based models fail to resolve small canopy clearings, which are evidently resolved by the pDSM-based models. Consistent with the quantitative results, the characteristic underprediction of tall canopies and the overprediction of small canopies is less pronounced for the pDSM-based models, most notably in areas A and C, where taller stands are present. The inclusion of spline coefficients leads to comparatively subtle visual changes for both the GEDI- and pDSM-based configurations, consistent with smaller quantitative improvements for the error metrics. Improvements can be observed for tall canopy heights (areas A and C) and small canopies (areas A and B), although the choice of reference data clearly has a bigger impact.

Overall, the visual results are consistent with the quantitative analysis. Although the DSM-Spline model performs best, fine-scale structures in highly heterogeneous areas, such as individual trees, are occasionally not correctly resolved (areas A and B), and the underprediction of tall canopies remains a persistent limitation, although much less pronounced than in the other models (areas A and D).

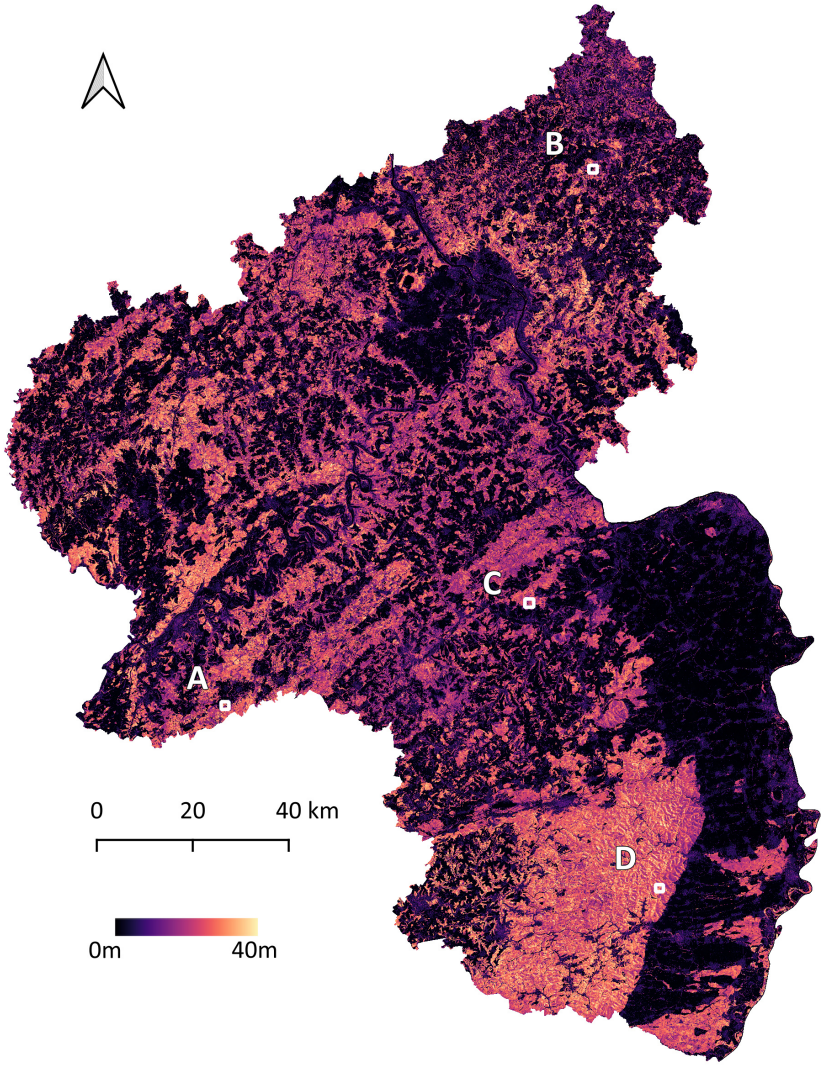


Figure 6: Height map for Rhineland-Palatinate based on pDSM data and spline coefficients for 2024. Areas of interest that will be further analyzed are highlighted.

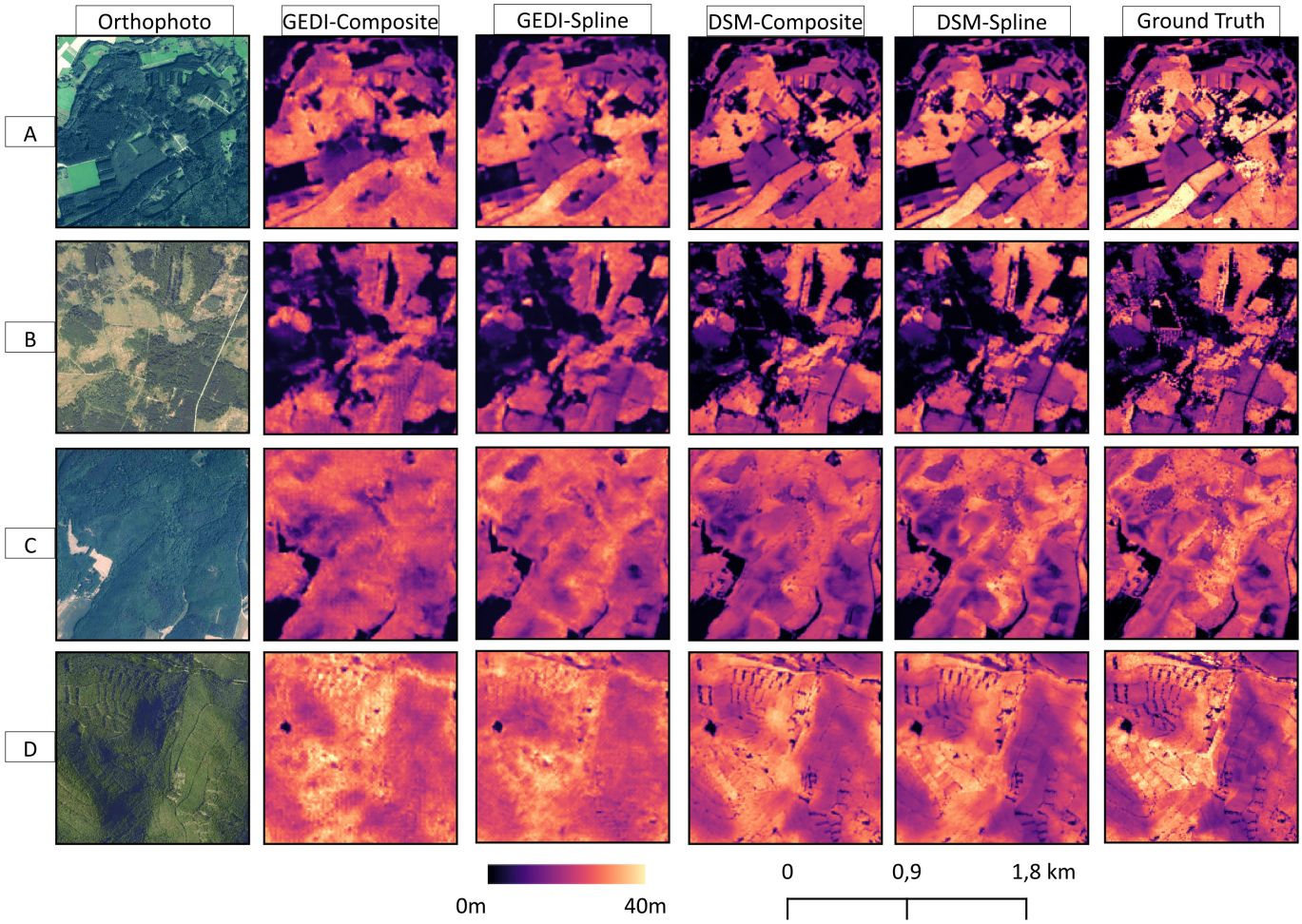


Figure 7: Visual comparison of height maps for different model configurations. The areas are taken from the spatial holdout for the years 2025 (A), 2024 (B), 2023 (C), 2022 (D), i.e., when validation data were available. The corresponding orthophotos have temporal offsets of ± 1 year. The ground truth is based on aDSM data.

The bin-wise annual growth analysis enables a detailed view of growth trends for forest areas that remained undisturbed between 2018 and 2025 (Figure 8). The highest annual growth rates between 2018 and 2021 were observed for the 5-10 m bin, whereas canopies between 0-5 m showed the largest growth between 2022 and 2025. Both bins showed median growth rates of approximately 0.3 - 1 m/year (Table A4). Taller bins consistently showed smaller growth, with the 25-30 m bin approximating an average growth of 0 m/year. For bins larger than 30 m, an increasingly negative growth can be observed. A consistent dip in growth can be observed for the year 2021 across most height bins, suggesting a year-specific modeling artifact.
Disturbed areas between 2019 and 2021 show substantially different height change trajectories between standing deadwood and other disturbances (Figure 9). When analyzing all standing deadwood within the study area, height reduction is delayed by approximately one year relative to other disturbances, which show a substantial height decline already within the disturbance year. Within the Hunsrück-Hochwald National Park, where salvage logging is not applied, standing deadwood instead shows a more gradual decline, converging with the height reduction observed for other disturbances approximately four years after the initial disturbance.

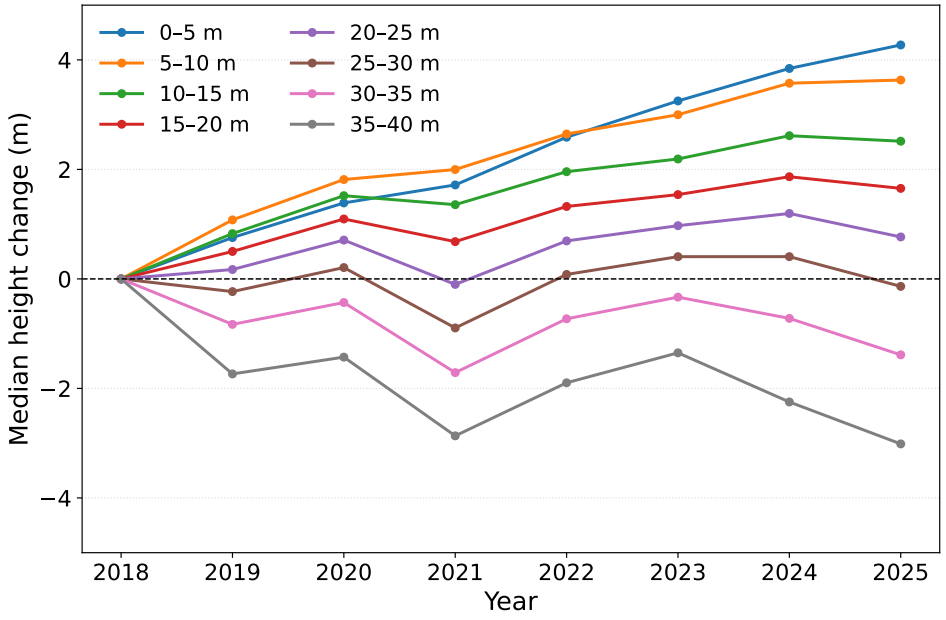


Figure 8: Annual growth of different canopy height bins. Growth is displayed as the median height change relative to the initial height of 2018. Only undisturbed pixels are displayed

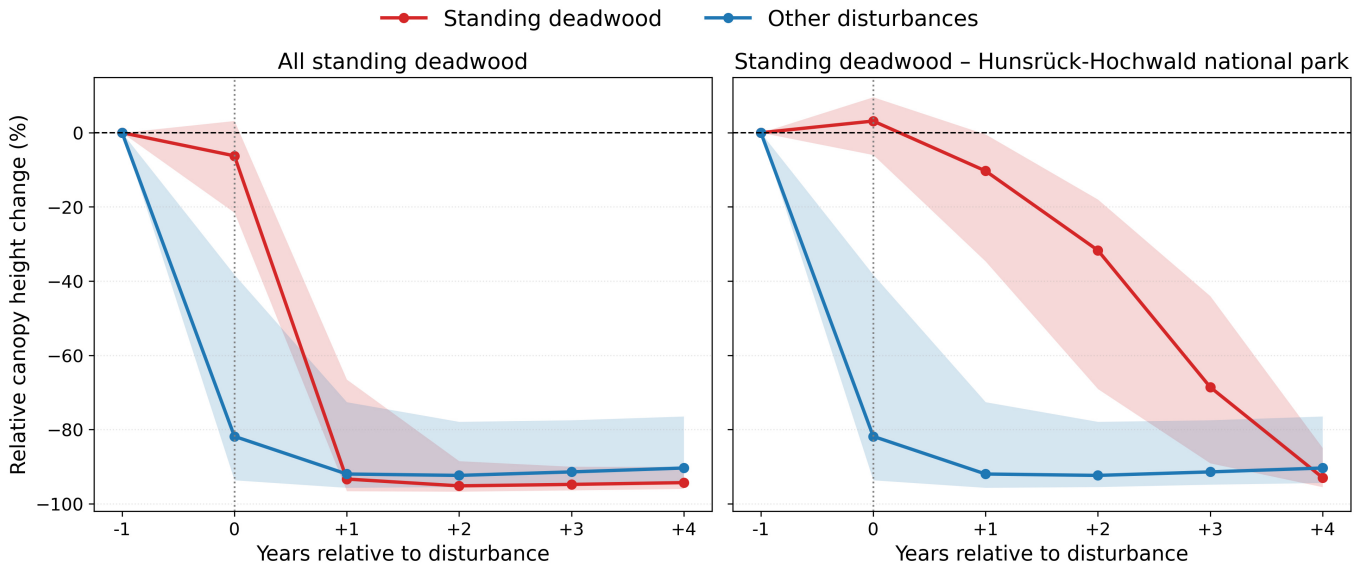


Figure 9: Height change for disturbed areas, relative to the disturbance time. Standing deadwood and other disturbances are differentiated. Standing deadwood is displayed for the entire study area and for the Hunsrück-Hochwald National Park only.

5.3 Comparison with existing Canopy Height maps

To assess our best performing model (pDSM-Spline) with respect to established canopy height products, we evaluated them with the aDSM data for 2020 used in this study (Figure A3). Our regionally-trained model performs best across all metrics and height bins. Improvements are most pronounced for smaller canopy heights when compared against GEDI-based products, which show error metrics broadly comparable to our GEDI-based configurations (Lang et al., 2023; Pauls et al., 2026) (Figure A4). Compared against Tolan et al. (2024), improvements are most substantial for taller canopies.

Visual comparison of the resulting maps further supports these findings, with our model resolving fine-scale structures and forest edges more clearly than the evaluated products, consistent with its higher accuracy for both short and tall canopies (Figure A5).

6 Discussion

Our study investigates the influence of different reference data sources and satellite data input representations on the modeling of multi-temporal canopy height. Both wall-to-wall pDSM training data and spline coefficients as input representations improved model accuracy substantially. A direct comparison of GEDI footprints and pDSM data against independent aDSM reference data confirms that this improvement is likely rooted in the inherent accuracy of the two reference sources themselves: pDSM data show a substantially better agreement with ALS (RMSE = 1.97 m, R^2 = 0.935) than the GEDI RH95 values (RMSE = 6.67 m, R^2 = 0.325) (Figure 10). This is consistent with previous findings, which highlight GEDI's sensitivity to geolocation errors and slope (Adam et al., 2020; H. Li et al., 2024; A. Liu et al., 2021). Notably, GEDI also inherently assigns a height of approximately 3 m to ground observations (Pauls et al., 2024), introducing an additional, systematic bias. Furthermore, GEDI-based canopy height maps are often trained on the top height of 25 m footprints, centered on a single 10 m pixel, providing no spatial context beyond the sparse footprint locations themselves (Dubayah et al., 2020; Lang et al., 2023). While the accuracy of GEDI-based models can be increased through extensive footprint filtering (Moudrỳ et al., 2024b) and adaptive loss functions (Pauls et al., 2024), the underlying limitations constitute an inherent constraint for any model trained on GEDI data, contributing to reduced achievable accuracy independent of model architecture or input representation. Interestingly, our GEDI-based configurations achieved higher accuracies against ALS data than the original GEDI data (RMSE = 5.98 m for GEDI-Composite and RMSE = 5.38 m for GEDI-Spline), which also has been observed in previous studies (Bermudez et al., 2026). This suggests that the model is, to a limited degree, able to compensate for GEDI's uncertainty, likely through spatial generalization over many training labels and spatial context from the input data.

The higher inherent precision of the pDSM labels likely also explains the substantial accuracy differences between the GEDI- and pDSM-based configurations. As the pDSM data have no inherent uncertainty concerning short tree heights and tends to resolve small-scale forest structure more precisely, gains in accuracy are substantial for small canopies. They furthermore provide wall-to-wall labels instead of GEDI's sparse labels, which may be particularly beneficial for CNN-based approaches, as the model can learn high-frequency spatial variation in canopy height between adjacent pixels (Lang et al., 2023). This dense coverage also results in a substantially larger number of valid supervised pixels per training chip compared to GEDI footprints, which may further contribute to the observed accuracy gains.

The pDSM and aDSM data differ in acquisition season: the pDSMs were mostly acquired under leaf-on conditions, whereas the aDSM data were acquired under leaf-off conditions. As leaf-off pulses penetrate deeper into deciduous crowns, this could bias the validation based on aDSM data. The close agreement between pDSM and aDSM (RMSE = 1.97 m, bias = 0.17 m) suggests that this effect is limited (Figure 10). As a residual influence cannot be fully excluded, leaf-on ALS data would be needed for quantification.

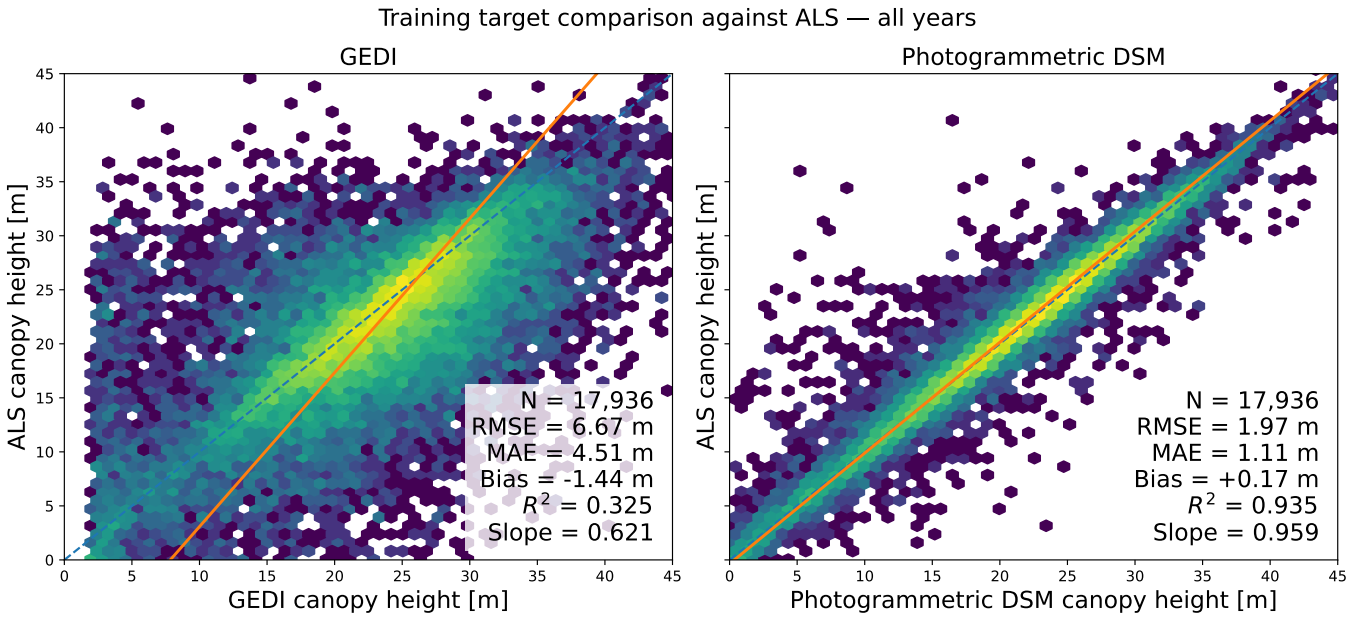


Figure 10: GEDI and photogrammetric DSM canopy height evaluated against aDSM reference data. Only pixels that have aDSM, pDSM and GEDI labels within specific years were included in the analysis. Error metrics are pooled across all years.

In addition to the choice of training data, the incorporation of Sentinel-2 spline coefficients also improved model accuracy substantially compared to median composites – regardless of reference data choice. Median composites select a single observation of the time series for each pixel and band, and hence effectively convert the rich multi-temporal information to a mono-temporal synthetic image. In addition, composites may be negatively affected by various factors such as the number of observations, radiometric consistency, or cloud artifacts (Francini et al., 2023), introducing spatial patterns that may be disadvantageous for CNN-based modeling. As they remain the basis for a variety of forest related remote sensing tasks such as disturbance and biomass monitoring (Francini et al., 2022; Senf & Seidl, 2021), as well as canopy height modeling (Pauls et al., 2024; Schwartz et al., 2024), they were chosen for the comparison within this study.
In contrast, the spline coefficients effectively preserve temporal information, such as phenology (Bolton et al., 2020), consequently yielding additional information for canopy height. They are also less susceptible to spatial artifacts from rapid land cover conversions, like harvesting or stand removal, which often appear in pixel-based compositing. Other time series-based feature representations such as harmonic regression coefficients (Wilson et al., 2018) or temporal embeddings from foundation models (Feng et al., 2026) have been shown to produce higher accuracies for forest related remote sensing tasks than composites or individual images, consistent with the findings in this study. Schug et al. (2026) found that spline coefficients exhibit high modeling accuracy when utilized for land cover fraction mapping. Compared to STMs and latent embeddings, they were characterized by the best accuracy, although embeddings resulted in a higher multi-annual stability when temporally transferring models. Nevertheless, their good performance in previous tasks, as well as efficient and comparatively fast computation motivated their selection as the temporal representation tested in this study.

Because the magnitude of improvements contributed by pDSM reference data and spline coefficients remained largely comparable across model configurations, this suggests that input and reference data improve modeling mostly independently rather than through strong synergistic effects. The improvement gained by the addition of spline coefficients was slightly larger for the pDSM-Spline configuration than for the GEDI-Spline configuration. This may be explained by the substantially lower inherent noise of the pDSM reference data compared to GEDI (RMSE against aDSM of 1.97 m and 6.67 m) (Figure 10). With less uncertainty

contained within the training labels, the model may be better able to exploit the additional temporal information provided by spline coefficients, which also hints at the possibility that optimized training parameters or architectural improvements of the deep learning model could yield additional gains in accuracy, as the remaining error can less likely be attributed to reference data quality. In some studies, Vision Transformer architectures have shown the potential to outperform classic CNN architectures for this task (Fayad et al., 2024; Sierra et al., 2026).

The underestimation of tall canopies remains a known limitation in canopy height modeling from satellite data (Moudrỳ et al., 2024a), which is likewise observed in our evaluation of the three global canopy height models (Figure A3 and A4). This effect is often attributed to saturation of the satellite signal and a low quantity of tall canopy training labels (Lang et al., 2023; Schwartz et al., 2024). The same pattern emerges in building height estimation from satellite imagery, where tall structures are likewise underestimated due to similar limitations (Cai et al., 2023; Frantz et al., 2021). This suggests that the underestimation of tall objects reflects a general challenge of height estimation from satellite data, rather than one specific to forests. In this study, both pDSM training labels and spline coefficient input representations reduced this error. This may be attributed to the fact that wall-to-wall training data provide more tall-canopy training samples as well as spatial context that can be beneficial when spectral differences in canopies become marginal. Frantz et al. (2023b) observed a similar pattern for building height, with saturation setting in at greater heights in the US compared to Germany (Frantz et al., 2021), which they partly attributed to the greater availability of tall training samples.
Additionally, Spline coefficients add beneficial phenological information that can further support this distinction. Choi et al. (2026) suggest that the benefit of multi-temporal satellite imagery for canopy height modeling can largely be attributed to tree species information. A similar mechanism may be observed with spline coefficients in this study, since the suitability of spline fitting for the mapping of tree species fractions has been shown (Klehr et al., 2025). We furthermore implemented a weighted loss function based on the error distribution of an initial, unweighted baseline model, to explicitly penalize errors for underrepresented height ranges such as tall canopies during training. Similar weighting strategies in canopy height modeling have shown to mitigate the underestimation of tall canopies successfully (Fayad et al., 2024). Although substantial improvements were achieved, the underestimation of tall canopies remains a persistent limitation across all model configurations. This is further reflected by the growth trend analysis, where canopies taller than 30 m partly showed declining height trends. Part of this phenomenon, might be caused by undetected disturbances within the disturbance product used for masking before the analysis – Thonfeld et al. (2026) report a user's accuracy of 92% for the disturbed class, i.e., 8% commission error. They further state that their approach is not able to detect loss of single trees, which could indicate the omission of areas affected by selective logging or naturally dying trees. Since scattered tree death can have a substantial influence on forest loss (Cheng et al., 2024), undetected logging, similarly affecting individual or small groups of trees, may contribute to the observed height reductions, especially since selective logging and crown defoliation are common within our study area, affecting mostly old trees (MKUEM, 2025).

Furthermore, the accuracy for short canopies was improved by the pDSM-spline model. This is consistent with findings that GEDI-based canopy height maps often severely overestimate short canopies (Dong et al., 2025; Moudrỳ et al., 2024a). The comparison against existing canopy height products supports this, where GEDI-based products showed the highest errors for small canopies, while Tolan et al. (2024), based on wall-to-wall ALS training data, showed comparatively smaller errors in this range. Improvements may partially also be attributed to the improved ability to resolve small canopy gaps and horizontal forest structure.
Overall, our pDSM-Spline configuration yielded better results across all metrics and heights compared to

the three evaluated global models. While parts of this can be attributed to improvements in input and training data, the comparison is also conducted between a highly localized model and global canopy height products, which inherently contributes to this advantage. Therefore, these results should not be overstated and rather be seen as an informative inter-comparison. Although the influence of both factors cannot be fully separated within the scope of this study, this may indicate that local or national models should be applied where precise canopy height information is required, consistent with studies explicitly comparing local and global model performance (Rolf et al., 2026). We do note however, that the global canopy height model of Pauls et al. (2026) shows comparable accuracy to our own GEDI models, highlighting the products robustness and the generalizability of their approach.

The multi-temporal error metrics showed comparatively stable values for unseen years across all model configurations, although the pDSM-Spline configuration showed the least inter-annual variability. This suggests that all configurations generalize reasonably well to years without training data, with pDSM-Spline showing the most consistent performance, and hence potential for temporal transfer, e.g., with respect to continuous monitoring. For applications such as growth monitoring, temporal stability becomes key. While the detailed temporal analysis of our best model (pDSM-Spline) revealed uncertainty and partially negative growth trends for canopies larger than 30 m, the overall results indicate realistic trends. The largest growth rates were observed for smaller canopy heights, decreasing with increasing tree height, which is consistent with known patterns of tree growth (Bontemps & Duplat, 2012; Duncanson & Dubayah, 2018). To mitigate the uncertainty in multi-temporal canopy height modeling, Pauls et al. (2026) enforced realistic growth trends through the usage of a growth loss. Implementing a similar approach could further improve the accuracy of growth trajectories and presents a promising direction for future research. However, this increases model complexity and potentially limits the detection of selective logging and gradual tree degradation, as reported by the authors. Hence, potential improvements will need to be balanced against practicability and applicability, requiring a targeted validation campaign for evaluation.

While the introduction of pDSM training data substantially improved modeling performance compared to GEDI footprints, this approach comes with its own set of limitations. First, high-quality DSM data are not available globally, which limits its applicability to regions with sufficient coverage. Within Europe, ALS and/or photogrammetric DSM coverage is generally good, although data availability, temporal coverage, acquisition parameters, and metadata vary considerably. In particular, national campaigns are often designed for surveying purposes and hence frequently conducted during leaf-off periods, making the data's applicability for vegetation structure suboptimal, especially for photogrammetric DSMs (Jayathunga et al., 2019; Moudrỳ et al., 2026). Despite these limitations, multiple recent state-wide campaigns for Germany (Hopfstock et al., 2022) and France (https://geoservices.ign.fr/lidarhd), as well as EU-wide open-data initiatives such as the INSPIRE directive (SDIU, 2007), aim to improve data availability. In this study, the approach was applied to an area with good pDSM and aDSM coverage; of these, aDSM was specifically reserved for validation, as it represents the data source with higher accuracy (Olofsson et al., 2014). This resulted in comparatively small validation sample sizes within the spatially held-out areas for some evaluated years (although still approximately 940,000 pixels at worst). However, the stability of results between different validation years indicates that this effect is limited.
We further acknowledge that the transferability of our model to other regions is likely limited to areas that show similar climatic and silvicultural conditions, and hence comprise a similar feature space (Meyer & Pebesma, 2021). The comparatively limited performance of the Tolan et al. (2024) product for our study area may also be explained by this limitation, since their model was calibrated primarily on ALS data from the continental US, which differs considerably from Europe's temperate forests. Spatial transferability of

the approach presented here therefore remains subject to future research. In a next step, we plan to apply the pDSM-spline modeling framework at the national scale across Germany.
The main limitations of using spline coefficients comprise data storage and computational demand. They require dense, corrected time series of satellite data, as well as sufficient computational capabilities during initial calculation, training and inference, given their comparatively heavy 220-band input. However, given the increasing prevalence of analysis ready data, e.g., through FORCE and its existing data cube on the German CODE-DE platform (Beyer et al., 2025; Frantz, 2019), the U.S. Analysis Ready Data program (Dwyer et al., 2018), the Harmonized Landsat & Sentinel-2 product (Claverie et al., 2018), or Google Earth Engine (Gorelick et al., 2017), along with current capabilities of cloud and high-performance computing, we do not consider this a major limitation. Furthermore, spline coefficients require less time and fewer resources to compute than learned embeddings from foundation models, and once computed, they can be reused across different downstream tasks. We additionally emphasize that all code used for this study is openly available and can be reused; please refer to the Data Availability section.

Since precise, temporally stable canopy height information is needed for various downstream tasks, we consider several potential applications for which the pDSM-Spline canopy height maps produced in this study are suitable inputs. A survey of forest practitioners found that respondents request errors below 3 m and a preference for data no older than five years (F. E. Fassnacht et al., 2025), underscoring the practical relevance of our annually updated, accurate pDSM-spline product (pooled RMSE = 3.14 m, MAE = 2.31 m). As this model performed considerably better for small canopies and showed temporal stability as well as realistic growth patterns, it may be applied for monitoring forest recovery, following disturbances and harvest. This could help with predicting future recovery based on ecological site conditions and inform foresters about the need for management interventions. Forest disturbances have increased significantly in Europe and are expected to increase further, making recovery monitoring increasingly relevant (Grünig et al., 2026; Senf & Seidl, 2021).
Furthermore, larger-scale maps based on this configuration may support the monitoring of biomass dynamics over time. Since canopy height is a key determinant of biomass (F. Fassnacht et al., 2014), precise height information may contribute to more accurate aboveground biomass estimates, leading to a better understanding of the role of forests in climate change mitigation.
We further note, that although we have focused on forests, the canopy height maps produced by our approach are a wall-to-wall products trained on a multi-purpose Digital Surface Model. As such, elevated objects outside of forests are similarly represented with predicted height values. We deliberately decided to not mask out these pixels, in support of other potential applications, e.g., applications related to building height in urban areas (Cai et al., 2023; Frantz et al., 2021). However, our product is not specifically validated outside of forests, which we considered to be out of scope of this study, remaining a direction for future research.
Beyond the applications discussed above, the results of this study also point to the potential usability of the produced canopy height maps for disturbance detection. As shown in the temporal analysis, pixels flagged as disturbed consistently showed substantial height decreases, hinting at the feasibility of a structure-based disturbance detection (Figure 9). The temporal analysis of standing deadwood further reveals that height loss for this disturbance type is delayed relative to other disturbances, due to salvage logging in the following year. Within unmanaged forests such as the Hunsrück-Hochwald National Park, this decline is much more gradual, indicating the time it takes for the standing deadwood to collapse. The example shown in Figure 11, depicting bark beetle disturbance followed by partial salvage logging, illustrates this contrast: salvage-logged areas are visually detectable as pronounced reductions in predicted canopy height, while standing deadwood is still characterized by heights similar to those of the intact stands. These findings

indicate that the temporal signature of height change may help distinguish between disturbance types such as standing deadwood and salvage-logged areas, representing a promising direction for future research, when combined with existing disturbance and mortality products (Schiefer et al., 2025; Thonfeld et al., 2026). Given the demonstrated advantages of our models, a similar approach applied at the national scale could feasibly extend applications such as recovery monitoring, biomass dynamics, and disturbance monitoring to a larger scale, provided suitable DSM training data are available.

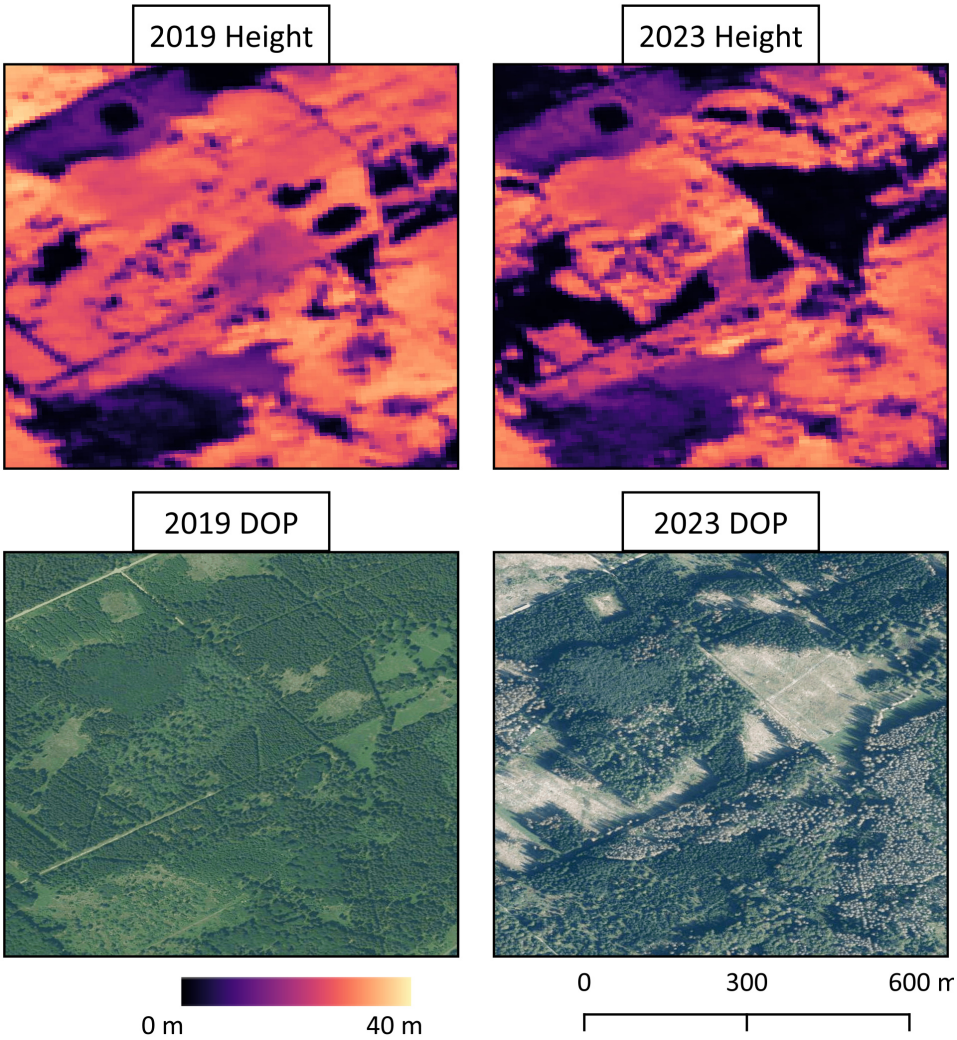


Figure 11: pDSM-Spline maps of Hunsrück-Hochwald Nationalpark, western Rhineland-Palatinate. Severe bark beetle attacks occurred between 2019 and 2023.

7 Conclusion

In this study, we investigated the influence of input feature representations and training data on canopy height modeling. This was done using four model configurations to assess the effect of training and input data. Both photogrammetric digital surface model (pDSM) training data and Sentinel-2 time series spline coefficients substantially increased modeling accuracy compared to GEDI training data and Sentinel-2 median composites. This demonstrates that time series information is a key feature for improving canopy height modeling accuracy, in addition to high-quality reference labels. Our results suggest that DSMs combined with temporal representations of satellite data should be the preferred setup for precise canopy height modeling, where such data are available. However, GEDI remains a valuable and practical reference source if DSMs are unavailable.

We found high temporal stability in our multi-annual predictions, suggesting suitability for various down-

stream applications such as disturbance monitoring, subsequent recovery monitoring, and biomass dynamics. Since this study focused on a relatively small research area, future work should focus on national, regional, or continental scales to assess transferability and the influence of patchy reference data availability. Lastly, the influence of canopy height models of higher accuracy on various downstream tasks should be explored, as well as the applicability of this modeling design to other structural target variables, such as canopy cover. Since canopy height remains a key structural indicator for forest carbon dynamics and climate-induced change, continued efforts to improve the accuracy and transferability of canopy height modeling will directly support adaptive forest monitoring.

Acknowledgments

This work was mainly supported by the PhD scholarship programme of the Deutsche Bundesstiftung Umwelt (DBU) (AZ: 20026/016). For parts of the work, FW received funding from the Forschungsanstalt für Waldökologie und Forstwirtschaft Rheinland-Pfalz under contract number FF53-02-2025. DK received funding from the Federal Ministry of Digital and Transport of the Federal Republic of Germany under contract number FKZ 50EW2408C.

Declaration of Competing Interests

The authors declare that they have no known competing financial interests or personal relationships that could have appeared to influence the work reported in this paper.

Data Availability

The code for the deep learning model used in this study is available on GitHub (https://github.com/FelixWengler/Sen2Height). The workflow for the spline coefficients is available on GitHub (https://github.com/ForestPulse/splinecoefs), as well as the TPE workflow (https://github.com/ForestPulse/thermal-time). The canopy height maps will be made available after review via Zenodo.

CRediT authorship contribution statement

Felix Wengler: Writing – original draft, Conceptualization, Visualization, Data curation, Software, Methodology, Validation, Formal analysis. **David Klehr:** Writing – review & editing, Methodology, Software, Data curation. **Alexander Wagner:** Resources, Supervision. **David Frantz:** Writing – review & editing, Methodology, Software, Conceptualization, Resources, Supervision.

Declaration of generative AI and AI-assisted technologies in the manuscript preparation process

During the preparation of this work, the author(s) used Claude in order to check for spelling and grammar mistakes, as well as sentence structure. After using this tool/service, the author(s) reviewed and edited the content as needed and take(s) full responsibility for the content of the published article.

References

Adam, M., Urbazaev, M., Dubois, C., & Schmullius, C. (2020). Accuracy assessment of gedi terrain elevation and canopy height estimates in european temperate forests: Influence of environmental and acquisition parameters. *Remote Sensing*, *12*(23), 3948. https://doi.org/10.3390/rs12233948

Bermudez, J., Rogers, C., Sothe, C., Cyr, D., & Gonsamo, A. (2026). An integrated deep learning approach to estimate canopy height and uncertainty by combining seasonal optical, sar and limited gedi lidar data over ontario's managed forests, canada. *Remote Sensing*, *18*(15), 2477. https://doi.org/10.3390/rs18152477

Beyer, F., Brandt, P., Schmidt, M., König, S., Stahl, U., Baumann, P., Golla, B., Gerighausen, H., & Möller, M. (2025). Big geodata and spatial data infrastructures: A perspective of a german authority. *PFG–Journal of Photogrammetry, Remote Sensing and Geoinformation Science*, 1–18. https://doi.org/10.1007/s41064-025-00351-0

Bolton, D. K., Gray, J. M., Melaas, E. K., Moon, M., Eklundh, L., & Friedl, M. A. (2020). Continental-scale land surface phenology from harmonized landsat 8 and sentinel-2 imagery. *Remote Sensing of Environment*, *240*, 111685. https://doi.org/10.1016/j.rse.2020.111685

Bontemps, J.-D., & Duplat, P. (2012). A non-asymptotic sigmoid growth curve for top height growth in forest stands. *Forestry: An International Journal of Forest Research*, *85*(3), 353–368. https://doi.org/10.1093/forestry/cps034

Braden, H. (1995). *The model AMBETI* (tech. rep.). Deutscher Wetterdienst. Offenbach am Main.

Buchner, J., Yin, H., Frantz, D., Kuemmerle, T., Askerov, E., Bakuradze, T., Bleyhl, B., Elizbarashvili, N., Komarova, A., Lewińska, K. E., et al. (2020). Land-cover change in the caucasus mountains since 1987 based on the topographic correction of multi-temporal landsat composites. *Remote Sensing of Environment*, *248*, 111967. https://doi.org/10.1016/j.rse.2020.111967

Cai, B., Shao, Z., Huang, X., Zhou, X., & Fang, S. (2023). Deep learning-based building height mapping using sentinel-1 and sentinel-2 data. *International Journal of Applied Earth Observation and Geoinformation*, *122*, 103399. https://doi.org/10.1016/j.jag.2023.103399

Chen, A., Cheng, K., Chen, Y., Qi, Z., Yang, H., Ren, Y., Yang, Z., Chen, M., Xu, J., Zhang, Y., et al. (2025). Validating recent global canopy height maps over china's forests based on uav lidar data. *Remote Sensing of Environment*, *329*, 114957. https://doi.org/10.1016/j.rse.2025.114957

Cheng, Y., Oehmcke, S., Brandt, M., Rosenthal, L., Das, A., Vrieling, A., Saatchi, S., Wagner, F., Mugabowindekwe, M., Verbruggen, W., et al. (2024). Scattered tree death contributes to substantial forest loss in california. *Nature communications*, *15*(1), 641. https://doi.org/10.1038/s41467-024-44991-z

Choi, C., Ryu, Y., Dechant, B., Yang, T., Wan, L., Jeong, S., & Wu, J. (2026). Species information in multi-temporal sentinel-2 data improves forest canopy height estimation. *Agricultural and Forest Meteorology*, *382*, 111114. https://doi.org/10.1016/j.agrformet.2026.111114

Cira, C.-I., Manso-Callejo, M.-Á., Alcarria, R., Iturrioz, T., & Arranz-Justel, J.-J. (2024). Insights into the effects of tile size and tile overlap levels on semantic segmentation models trained for road surface area extraction from aerial orthophotography. *Remote Sensing*, *16*(16), 2954. https://doi.org/10.3390/rs16162954

Claverie, M., Ju, J., Masek, J. G., Dungan, J. L., Vermote, E. F., Roger, J.-C., Skakun, S. V., & Justice, C. (2018). The harmonized landsat and sentinel-2 surface reflectance data set. *Remote sensing of environment*, *219*, 145–161. https://doi.org/10.1016/j.rse.2018.09.002

Coops, N. C., Tompalski, P., Goodbody, T. R., Queinnec, M., Luther, J. E., Bolton, D. K., White, J. C., Wulder, M. A., van Lier, O. R., & Hermosilla, T. (2021). Modelling lidar-derived estimates of for-

est attributes over space and time: A review of approaches and future trends. *Remote Sensing of Environment*, *260*, 112477. https://doi.org/10.1016/j.rse.2021.112477

Copernicus Land Monitoring Service. (2020). *Dominant leaf type 2018 (raster 10 m), europe*. https://doi.org/10.2909/82f93572-9888-47ef-97a1-5cac5985a26a

De Keersmaecker, W., Verhegghen, A., Bertels, L., Senf, C., Viana-Soto, A., Verkerk, P. J., Zanaga, D., & Van De Kerchove, R. (2026). Mapping forest canopy height over europe by integrating sentinel-1, sentinel-2, gedi, and icesat-2 data. *Earth System Science Data Discussions*, *2026*, 1–21. https://doi.org/10.5194/essd-2026-329

Dong, H., Xu, Z., Wu, J., Lan, T., Wang, L., Shao, G., & Tang, L. (2025). High-precision airborne lidar remains essential for urban forestry: Revealing the limitations of recent large-scale canopy height products in urban contexts. *International Journal of Applied Earth Observation and Geoinformation*, *143*, 104791. https://doi.org/10.1016/j.jag.2025.104791

Drusch, M., Del Bello, U., Carlier, S., Colin, O., Fernandez, V., Gascon, F., Hoersch, B., Isola, C., Laberinti, P., Martimort, P., et al. (2012). Sentinel-2: Esa's optical high-resolution mission for gmes operational services. *Remote sensing of Environment*, *120*, 25–36. https://doi.org/10.1016/j.rse.2011.11.026

Dubayah, R., Blair, J. B., Goetz, S., Fatoyinbo, L., Hansen, M., Healey, S., Hofton, M., Hurtt, G., Kellner, J., Luthcke, S., et al. (2020). The global ecosystem dynamics investigation: High-resolution laser ranging of the earth's forests and topography. *Science of remote sensing*, *1*, 100002. https://doi.org/10.1016/j.srs.2020.100002

Duncanson, L., & Dubayah, R. (2018). Monitoring individual tree-based change with airborne lidar. *Ecology and evolution*, *8*(10), 5079–5089. https://doi.org/10.1002/ece3.4075

DWD – German Meteorological Service. (2026). *Open data server of the german meteorological service*. Retrieved August 26, 2026, from https://opendata.dwd.de/climate_environment/CDC/grids_germany/daily/soil_temperature_5cm/

Dwyer, J. L., Roy, D. P., Sauer, B., Jenkerson, C. B., Zhang, H. K., & Lymburner, L. (2018). Analysis ready data: Enabling analysis of the landsat archive. *Remote Sensing*, *10*(9), 1363. https://doi.org/10.3390/rs10091363

Fassnacht, F. E., Mager, C., Waser, L. T., Kanjir, U., Schäfer, J., Buhvald, A. P., Shafeian, E., Schiefer, F., Stančič, L., Immitzer, M., et al. (2025). Forest practitioners' requirements for remote sensing-based canopy height, wood-volume, tree species, and disturbance products. *Forestry: An International Journal of Forest Research*, *98*(2), 233–252. https://doi.org/10.1093/forestry/cpae021

Fassnacht, F., Hartig, F., Latifi, H., Berger, C., Hernández, J., Corvalán, P., & Koch, B. (2014). Importance of sample size, data type and prediction method for remote sensing-based estimations of aboveground forest biomass. *Remote sensing of environment*, *154*, 102–114. https://doi.org/10.1016/j.rse.2014.07.028

Fayad, I., Ciais, P., Schwartz, M., Wigneron, J.-P., Baghdadi, N., de Truchis, A., d'Aspremont, A., Frappart, F., Saatchi, S., Sean, E., et al. (2024). Hy-tec: A hybrid vision transformer model for high-resolution and large-scale mapping of canopy height. *Remote Sensing of Environment*, *302*, 113945. https://doi.org/10.1016/j.rse.2023.113945

Feng, Z., Atzberger, C., Jaffer, S., Knezevic, J., Sormunen, S., Young, R., Lisaius, M. C., Immitzer, M., Jackson, T., Ball, J., et al. (2026). Tessera: Temporal embeddings of surface spectra for earth representation and analysis. *Proceedings of the IEEE/CVF Conference on Computer Vision and Pattern Recognition*, 34818–34831. https://doi.org/10.48550/arXiv.2506.203800

Francini, S., D'Amico, G., Vangi, E., Borghi, C., & Chirici, G. (2022). Integrating gedi and landsat: Spaceborne lidar and four decades of optical imagery for the analysis of forest disturbances and biomass changes in italy. *Sensors*, *22*(5), 2015. https://doi.org/10.3390/s22052015

Francini, S., Hermosilla, T., Coops, N. C., Wulder, M. A., White, J. C., & Chirici, G. (2023). An assessment approach for pixel-based image composites. *ISPRS Journal of Photogrammetry and Remote Sensing*, *202*, 1–12. https://doi.org/10.1016/j.isprsjprs.2023.06.002

Frantz, D. (2019). Force—landsat+ sentinel-2 analysis ready data and beyond. *Remote Sensing*, *11*(9), 1124. https://doi.org/10.3390/rs11091124

Frantz, D., Haß, E., Uhl, A., Stoffels, J., & Hill, J. (2018). Improvement of the Fmask algorithm for Sentinel-2 images: Separating clouds from bright surfaces based on parallax effects. *Remote sensing of environment*, *215*, 471–481. https://doi.org/10.1016/j.rse.2018.04.046

Frantz, D., Röder, A., Stellmes, M., & Hill, J. (2016a). An operational radiometric landsat preprocessing framework for large-area time series applications. *IEEE Transactions on Geoscience and Remote Sensing*, *54*(7), 3928–3943. https://doi.org/10.1109/TGRS.2016.2530856

Frantz, D., Rufin, P., Janz, A., Ernst, S., Pflugmacher, D., Schug, F., & Hostert, P. (2023a). Understanding the robustness of spectral-temporal metrics across the global landsat archive from 1984 to 2019–a quantitative evaluation. *Remote Sensing of Environment*, *298*, 113823. https://doi.org/10.1016/j.rse.2023.113823

Frantz, D., Schug, F., Okujeni, A., Navacchi, C., Wagner, W., van der Linden, S., & Hostert, P. (2021). National-scale mapping of building height using sentinel-1 and sentinel-2 time series. *Remote Sensing of Environment*, *252*, 112128. https://doi.org/https://doi.org/10.1016/j.rse.2020.112128

Frantz, D., Schug, F., Wiedenhofer, D., Baumgart, A., Virág, D., Cooper, S., Gómez-Medina, C., Lehmann, F., Udelhoven, T., van der Linden, S., et al. (2023b). Unveiling patterns in human dominated landscapes through mapping the mass of us built structures. *Nature Communications*, *14*(1), 8014. https://doi.org/10.1038/s41467-023-43755-5

Frantz, D., Stellmes, M., Röder, A., Udelhoven, T., Mader, S., & Hill, J. (2016b). Improving the spatial resolution of land surface phenology by fusing medium-and coarse-resolution inputs. *IEEE Transactions on Geoscience and Remote Sensing*, *54*(7), 4153–4164. https://doi.org/10.1109/TGRS.2016.2537929

Gauer, J. (2012). Waldökologische Naturräume Deutschlands-Forstliche Wuchsgebiete und Wuchsbezirke: Digitale topographische Grundlagen-Neubearbeitung Stand 2011.

Gorelick, N., Hancher, M., Dixon, M., Ilyushchenko, S., Thau, D., & Moore, R. (2017). Google earth engine: Planetary-scale geospatial analysis for everyone. *Remote sensing of Environment*, *202*, 18–27. https://doi.org/10.1016/j.rse.2017.06.031

Griffiths, P., van der Linden, S., Kuemmerle, T., & Hostert, P. (2013). A pixel-based landsat compositing algorithm for large area land cover mapping. *IEEE Journal of Selected Topics in Applied Earth Observations and Remote Sensing*, *6*(5), 2088–2101. https://doi.org/10.1109/JSTARS.2012.2228167

Grünig, M., Rammer, W., Senf, C., Albrich, K., André, F., Augustynczik, A. L., Baumann, M., Bohn, F. J., Bouwman, M., Bugmann, H., et al. (2026). Climate change will increase forest disturbances in europe throughout the 21st century. *Science*, *391*(6789), eadx6329. https://doi.org/10.1126/science.adx6329

Haala, N. (2011). Multiray photogrammetry and dense image matching. *Photogrammetric week*, *11*, 185–195.

He, K., Zhang, X., Ren, S., & Sun, J. (2016). Deep residual learning for image recognition. *Proceedings of the IEEE conference on computer vision and pattern recognition*, 770–778. https://doi.org/10.48550/arXiv.1512.03385

Hodson, T. O. (2022). Root mean square error (rmse) or mean absolute error (mae): When to use them or not. *Geoscientific Model Development Discussions*, *2022*, 1–10.

Hopfstock, A., Knöfel, P., & Lindl, F. (2022). Digital twin germany–a digital replica for simulation and analysis build on geospatial data. *Abstracts of the ICA*, *5*, 119.

Jayathunga, S., Owari, T., & Tsuyuki, S. (2019). Digital aerial photogrammetry for uneven-aged forest management: Assessing the potential to reconstruct canopy structure and estimate living biomass. *Remote Sensing*, *11*(3), 338. https://doi.org/10.3390/rs11030338

Kacic, P., Thonfeld, F., Gessner, U., & Kuenzer, C. (2023). Forest structure characterization in germany: Novel products and analysis based on gedi, sentinel-1 and sentinel-2 data. *Remote Sensing*, *15*(8), 1969. https://doi.org/10.3390/rs15081969

Kalinicheva, E., Helen, F., Mermoz, S., Mouret, F., & Planells, M. (2026). Super-resolved canopy height mapping from sentinel-2 time series using airborne lidar hd reference data across metropolitan france. *Remote Sensing of Environment*, *344*, 115536. https://doi.org/10.1016/j.rse.2026.115536

Kingma, D. P., & Ba, J. (2014). Adam: A method for stochastic optimization. *arXiv preprint arXiv:1412.6980*. https://doi.org/10.48550/arXiv.1412.6980

Klehr, D., Stoffels, J., Hill, A., Pham, V.-D., van der Linden, S., & Frantz, D. (2025). Mapping tree species fractions in temperate mixed forests using sentinel-2 time series and synthetically mixed training data. *Remote Sensing of Environment*, *323*, 114740. https://doi.org/10.1016/j.rse.2025.114740

Landesforsten Rheinland-Pfalz. (2022). Unser Wald in Rheinland-Pfalz - Ergebnisse der Bundeswaldinventur 4. https://www.wald.rlp.de/wald/beeindruckende-zahlen/bundeswaldinventur

Lang, N., Jetz, W., Schindler, K., & Wegner, J. D. (2023). A high-resolution canopy height model of the earth. *Nature Ecology & Evolution*, *7*(11), 1778–1789. https://doi.org/10.1038/s41559-023-02206-6

Li, H., Li, X., Kato, T., Hayashi, M., Fu, J., & Hiroshima, T. (2024). Accuracy assessment of gedi terrain elevation, canopy height, and aboveground biomass density estimates in japanese artificial forests. *Science of Remote Sensing*, *10*, 100144. https://doi.org/10.1016/j.srs.2024.100144

Li, R., Zheng, S., Duan, C., Wang, L., & Zhang, C. (2022). Land cover classification from remote sensing images based on multi-scale fully convolutional network. *Geo-spatial information science*, *25*(2), 278–294. https://doi.org/10.1080/10095020.2021.2017237

Liu, A., Cheng, X., & Chen, Z. (2021). Performance evaluation of gedi and icesat-2 laser altimeter data for terrain and canopy height retrievals. *Remote sensing of environment*, *264*, 112571. https://doi.org/10.1016/j.rse.2021.112571

Liu, S., Brandt, M., Nord-Larsen, T., Chave, J., Reiner, F., Lang, N., Tong, X., Ciais, P., Igel, C., Pascual, A., et al. (2023). The overlooked contribution of trees outside forests to tree cover and woody biomass across europe. *Science advances*, *9*(37), eadh4097. https://doi.org/10.1126/sciadv.adh4097

LVermGeoRLP. (2026). Geodaten des Landes Rheinland-Pfalz [Datenlizenz Deutschland – Namensnennung – Version 2.0 (dl-de/by-2-0)]. https://metaportal.rlp.de/gui/html/3d2dda7d-b4b5-47d2-b074-dd45edd36738

Meyer, H., & Pebesma, E. (2021). Predicting into unknown space? estimating the area of applicability of spatial prediction models. *Methods in Ecology and Evolution*, *12*(9), 1620–1633. https://doi.org/10.1111/2041-210X.13650

Meyer, H., Reudenbach, C., Hengl, T., Katurji, M., & Nauss, T. (2018). Improving performance of spatio-temporal machine learning models using forward feature selection and target-oriented validation. *Environmental Modelling & Software*, *101*, 1–9. https://doi.org/10.1016/j.envsoft.2017.12.001

MKUEM. (2025). *Waldzustandsbericht 2025*. Ministerium für Klimaschutz, Umwelt, Energie und Mobilität. Mainz. https://fawf.wald.rlp.de/de/veroeffentlichungen/waldzustandsbericht/

Moudrỳ, V., Gábor, L., Marselis, S., Pracná, P., Barták, V., Prošek, J., Navrátilová, B., Novotnỳ, J., Potčková, M., Gdulová, K., et al. (2024a). Comparison of three global canopy height maps and their applicability to biodiversity modeling: Accuracy issues revealed. *Ecosphere*, *15*(10), e70026. https://doi.org/10.1002/ecs2.70026

Moudrỳ, V., Prošek, J., Marselis, S., Marešová, J., Šárovcová, E., Gdulová, K., Kozhoridze, G., Torresani, M., Rocchini, D., Eltner, A., et al. (2024b). How to find accurate terrain and canopy height gedi footprints in temperate forests and grasslands? *Earth and Space Science*, *11*(10), e2024EA003709. https://doi.org/10.1029/2024EA003709

Moudrỳ, V., Remelgado, R., Forkel, M., Torresani, M., Laurin, G. V., Šárovcová, E., Garcia Millan, V. E., Fischer, F. J., Jucker, T., Gallay, M., et al. (2026). Spaceborne canopy height products should be complemented with airborne laser scanning data: Toward a european canopy height model. *Earth and Space Science*, *13*(1), e2025EA004544. https://doi.org/10.1029/2025EA004544

Nunes, L. J., Meireles, C. I., Pinto Gomes, C. J., & Almeida Ribeiro, N. M. (2020). Forest contribution to climate change mitigation: Management oriented to carbon capture and storage. *Climate*, *8*(2), 21. https://doi.org/10.3390/cli8020021

Nurminen, K., Karjalainen, M., Yu, X., Hyyppä, J., & Honkavaara, E. (2013). Performance of dense digital surface models based on image matching in the estimation of plot-level forest variables. *ISPRS Journal of photogrammetry and Remote Sensing*, *83*, 104–115. https://doi.org/10.1016/j.isprsjprs.2013.06.005

Nyborg, J., Pelletier, C., & Assent, I. (2022). Generalized classification of satellite image time series with thermal positional encoding. *2022 IEEE/CVF Conference on Computer Vision and Pattern Recognition Workshops (CVPRW)*, 1391–1401. https://doi.org/10.1109/CVPRW56347.2022.00145

Oktay, O., Schlemper, J., Folgoc, L. L., Lee, M., Heinrich, M., Misawa, K., Mori, K., McDonagh, S., Hammerla, N. Y., Kainz, B., et al. (2018). Attention u-net: Learning where to look for the pancreas. *arXiv preprint arXiv:1804.03999*. https://doi.org/10.48550/arXiv.1804.03999

Olofsson, P., Foody, G. M., Herold, M., Stehman, S. V., Woodcock, C. E., & Wulder, M. A. (2014). Good practices for estimating area and assessing accuracy of land change. *Remote sensing of Environment*, *148*, 42–57. https://doi.org/10.1016/j.rse.2014.02.015

Pan, Y., Birdsey, R. A., Phillips, O. L., & Jackson, R. B. (2013). The structure, distribution, and biomass of the world's forests. *Annual review of ecology, evolution, and systematics*, *44*(1), 593–622. https://doi.org/10.1146/annurev-ecolsys-110512-135914

Paszke, A., Gross, S., Massa, F., Lerer, A., Bradbury, J., Chanan, G., Killeen, T., Lin, Z., Gimelshein, N., Antiga, L., et al. (2019). Pytorch: An imperative style, high-performance deep learning library. *Advances in neural information processing systems*, *32*. https://doi.org/10.48550/arXiv.1912.01703

Pauls, J., Schrödter, K., Ligensa, S., Schwartz, M., Turan, B., Zimmer, M., Saatchi, S., Pokutta, S., Ciais, P., & Gieseke, F. (2026). Echosat: Estimating canopy height over space and time. *arXiv preprint arXiv:2602.21421*. https://doi.org/10.48550/arXiv.2602.21421

Pauls, J., Zimmer, M., Kelly, U. M., Schwartz, M., Saatchi, S., Ciais, P., Pokutta, S., Brandt, M., & Gieseke, F. (2024). Estimating canopy height at scale. *arXiv preprint arXiv:2406.01076*. https://doi.org/10.48550/arXiv.2406.01076

Potapov, P., Li, X., Hernandez-Serna, A., Tyukavina, A., Hansen, M. C., Kommareddy, A., Pickens, A., Turubanova, S., Tang, H., Silva, C. E., et al. (2021). Mapping global forest canopy height through integration of gedi and landsat data. *Remote Sensing of Environment*, *253*, 112165. https://doi.org/10.1016/j.rse.2020.112165

Rolf, E., Gordon, L., Tambe, M., & Davies, A. (2026). Contrasting local and global modeling with machine learning and satellite data: A case study estimating tree canopy height in african savannas. *Journal of Machine Learning Research*, *27*(45), 1–37. https://doi.org/10.48550/arXiv.2411.14354

Ronneberger, O., Fischer, P., & Brox, T. (2015). U-net: Convolutional networks for biomedical image segmentation. *International Conference on Medical image computing and computer-assisted intervention*, 234–241. https://doi.org/10.1007/978-3-319-24574-4_28

Roy, D. P., Li, Z., & Zhang, H. K. (2017). Adjustment of sentinel-2 multi-spectral instrument (msi) red-edge band reflectance to nadir brdf adjusted reflectance (nbar) and quantification of red-edge band brdf effects. *Remote Sensing*, *9*(12), 1325. https://doi.org/10.3390/rs9121325

Schiefer, F., Schmidtlein, S., Hartmann, H., Schnabel, F., & Kattenborn, T. (2025). Large-scale remote sensing reveals that tree mortality in germany appears to be greater than previously expected. *Forestry: An International Journal of Forest Research*, *98*(4), 535–549. https://doi.org/10.1093/forestry/cpae062

Schug, F., Klehr, D., Mahler, J., & Frantz, D. (2026). Multi-annual sub-pixel land cover mapping with tessera latent embeddings. *Earth ArXiv preprint*. https://doi.org/10.31223/X59J7C

Schwartz, M., Ciais, P., De Truchis, A., Chave, J., Ottlé, C., Vega, C., Wigneron, J.-P., Nicolas, M., Jouaber, S., Liu, S., et al. (2023). Forms: Forest multiple source height, wood volume, and biomass maps in france at 10 to 30 m resolution based on sentinel-1, sentinel-2, and global ecosystem dynamics investigation (gedi) data with a deep learning approach. *Earth System Science Data*, *15*(11), 4927–4945. https://doi.org/10.5194/essd-15-4927-2023

Schwartz, M., Ciais, P., Ottlé, C., De Truchis, A., Vega, C., Fayad, I., Brandt, M., Fensholt, R., Baghdadi, N., Morneau, F., et al. (2024). High-resolution canopy height map in the landes forest (france) based on gedi, sentinel-1, and sentinel-2 data with a deep learning approach. *International Journal of Applied Earth Observation and Geoinformation*, *128*, 103711. https://doi.org/10.1016/j.jag.2024.103711

SDIU. (2007). Inspire: An innovative approach to the development of spatial data infrastructures in europe. *Research and theory in advancing spatial data infrastructure concepts*, 93.

Senf, C., Müller, J., & Seidl, R. (2019). Post-disturbance recovery of forest cover and tree height differ with management in central europe. *Landscape Ecology*, *34*(12), 2837–2850. https://doi.org/10.1007/s10980-019-00921-9

Senf, C., & Seidl, R. (2021). Mapping the forest disturbance regimes of europe. *Nature sustainability*, *4*(1), 63–70. https://doi.org/10.1038/s41893-020-00609-y

Sierra, S., Ramo, R., Padilla, M., & Cobo, A. (2026). Assessing the impact of lidar density and input features on forest canopy height estimation through xgboost, cnn, and cnn+ transformer approaches. *Remote Sensing*, *18*(4), 584. https://doi.org/10.3390/rs18040584

Tang, H., Stoker, J., Luthcke, S., Armston, J., Lee, K., Blair, B., & Hofton, M. (2023). Evaluating and mitigating the impact of systematic geolocation error on canopy height measurement performance of gedi. *Remote Sensing of Environment*, *291*, 113571. https://doi.org/10.1016/j.rse.2023.113571

Thonfeld, F., Kacic, P., Holzwarth, S., Wegler, M., Asam, S., & Kuenzer, C. (2026). Forest canopy cover loss dynamics in germany between 2017 and 2024: Revealing regional differences. *International Journal of Applied Earth Observation and Geoinformation*, *146*, 105157. https://doi.org/10.1016/j.jag.2026.105157

Tolan, J., Yang, H.-I., Nosarzewski, B., Couairon, G., Vo, H. V., Brandt, J., Spore, J., Majumdar, S., Haziza, D., Vamaraju, J., et al. (2024). Very high resolution canopy height maps from rgb imagery using self-supervised vision transformer and convolutional decoder trained on aerial lidar. *Remote Sensing of Environment*, *300*, 113888. https://doi.org/10.1016/j.rse.2023.113888

Torres, R., Snoeij, P., Geudtner, D., Bibby, D., Davidson, M., Attema, E., Potin, P., Rommen, B., Floury, N., Brown, M., et al. (2012). Gmes sentinel-1 mission. *Remote sensing of environment*, *120*, 9–24. https://doi.org/10.1016/j.rse.2011.05.028

Turubanova, S., Potapov, P., Hansen, M. C., Li, X., Tyukavina, A., Pickens, A. H., Hernandez-Serna, A., Arranz, A. P., Guerra-Hernandez, J., Senf, C., et al. (2023). Tree canopy extent and height change in europe, 2001–2021, quantified using landsat data archive. *Remote Sensing of Environment*, *298*, 113797. https://doi.org/10.1016/j.rse.2023.113797

Wilson, B. T., Knight, J. F., & McRoberts, R. E. (2018). Harmonic regression of landsat time series for modeling attributes from national forest inventory data. *ISPRS journal of Photogrammetry and Remote Sensing*, *137*, 29–46. https://doi.org/10.1016/j.isprsjprs.2018.01.006

Wu, Y., & He, K. (2018). Group normalization. *Proceedings of the European conference on computer vision (ECCV)*, 3–19. https://doi.org/10.48550/arXiv.1803.08494

Supplementary Material

Multi-temporal Canopy Height Modeling using Deep Learning and Sentinel-2: The Influence of Training Data and Input Feature Representations

Felix Wengler, David Klehr, Alexander Wagner, David Frantz*

*Corresponding author

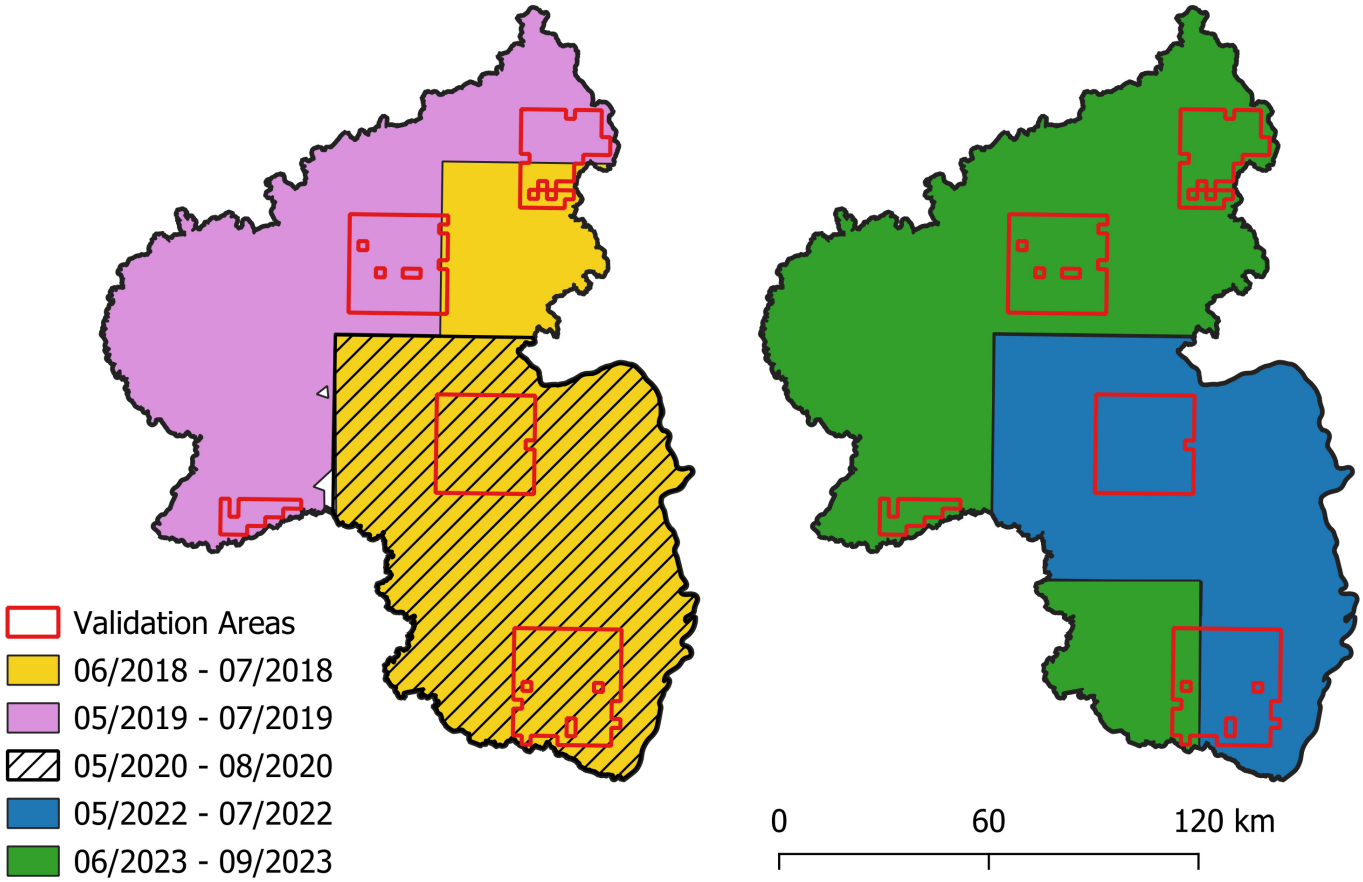


Figure A1: Spatiotemporal coverage of photogrammetric DSM training data for the years 2018-2020 and 2022-2023. Validation areas are marked in red.

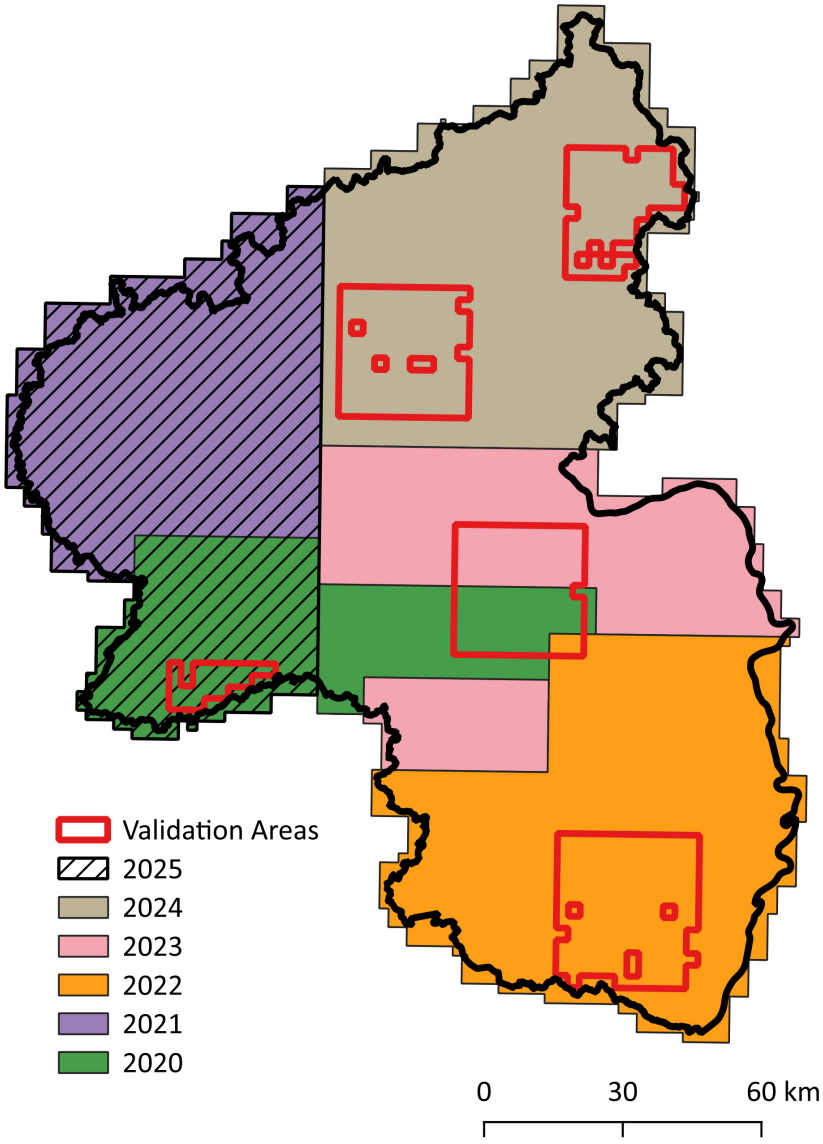


Figure A2: Spatiotemporal coverage of independent ALS validation data for the years 2020-2025. Validation areas are marked in red.

Table A1: Available training and validation chips per year for both GEDI and pDSM reference data sources.

Year	pDSM Train	pDSM Val	GEDI Train	GEDI Val
2018	959	229	0	0
2019	645	164	821	146
2020	749	199	1091	202
2021	0	0	833	206
2022	641	198	980	266
2023	1038	228	0	0
2024	0	0	1014	270

Table A4: Median annual canopy-height change for undisturbed areas of pDSM-Spline model by initial canopy-height bin and year pair. Changes are reported in m.

Height bin	**Year pair**	**Median annual change in m**
0–5 m	2018–2019	0.71
	2019–2020	0.45

Height class	Year pair	Median annual change [m yr^{-1}]
	2020–2021	0.22
	2021–2022	0.74
	2022–2023	0.53
	2023–2024	0.49
	2024–2025	0.40
5–10 m	2018–2019	0.99
	2019–2020	0.59
	2020–2021	0.10
	2021–2022	0.60
	2022–2023	0.33
	2023–2024	0.51
	2024–2025	0.14
10–15 m	2018–2019	0.76
	2019–2020	0.64
	2020–2021	-0.17
	2021–2022	0.59
	2022–2023	0.19
	2023–2024	0.47
	2024–2025	-0.08
15–20 m	2018–2019	0.46
	2019–2020	0.60
	2020–2021	-0.48
	2021–2022	0.70
	2022–2023	0.24
	2023–2024	0.30
	2024–2025	-0.25
20–25 m	2018–2019	0.13
	2019–2020	0.55
	2020–2021	-0.85
	2021–2022	0.87
	2022–2023	0.21
	2023–2024	0.23
	2024–2025	-0.43
25–30 m	2018–2019	-0.23
	2019–2020	0.51
	2020–2021	-1.08
	2021–2022	0.96
	2022–2023	0.29
	2023–2024	0.02
	2024–2025	-0.58
30–35 m	2018–2019	-0.80
	2019–2020	0.48
	2020–2021	-1.32

Height class	Year pair	Median annual change [m yr^{-1}]
	2021–2022	1.01
	2022–2023	0.37
	2023–2024	-0.35
	2024–2025	-0.70
35–40 m	2018–2019	-1.70
	2019–2020	0.40
	2020–2021	-1.45
	2021–2022	0.92
	2022–2023	0.49
	2023–2024	-0.76
	2024–2025	-0.79

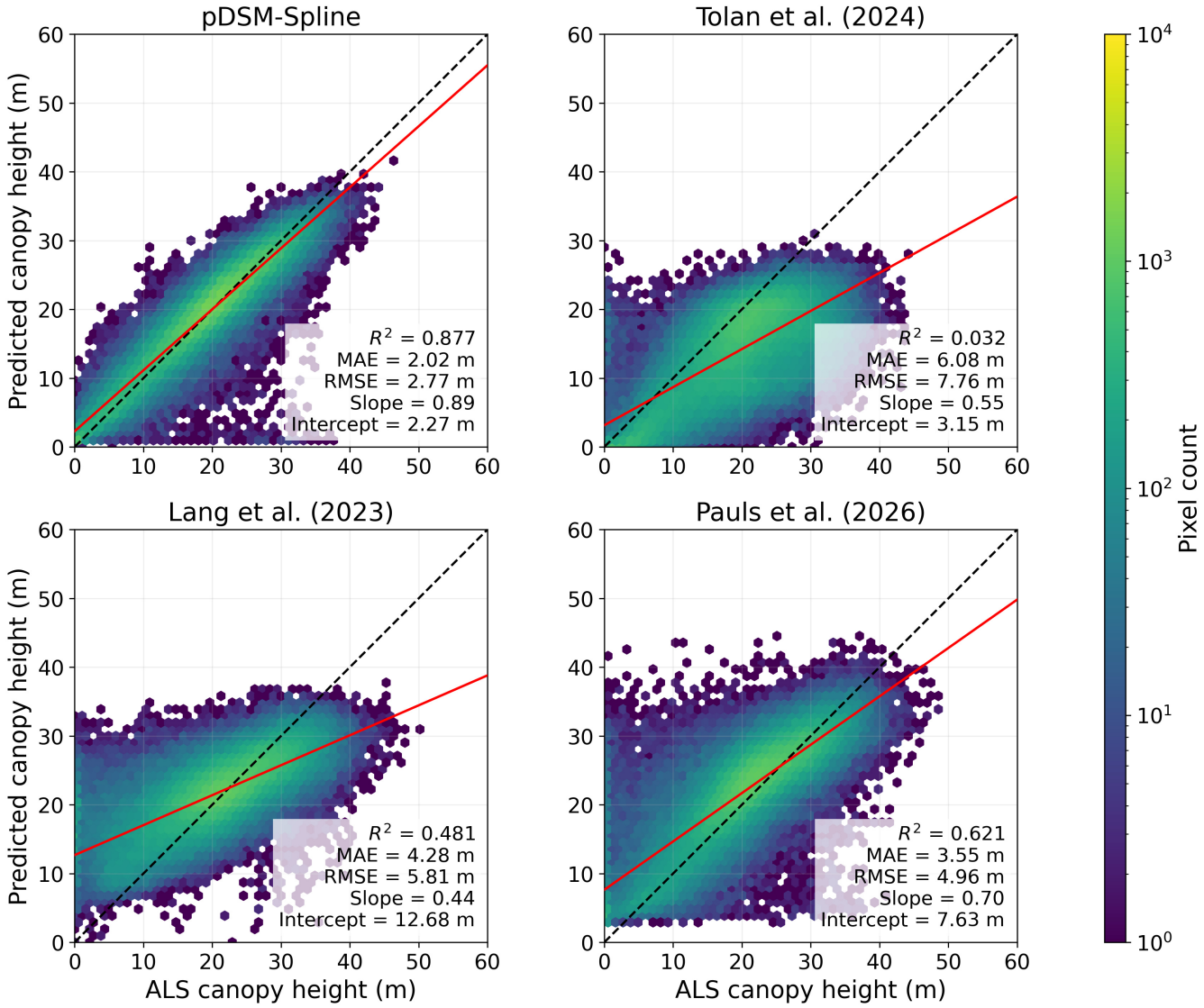


Figure A3: Comparison of our pDSM-Spline model against global canopy height products for the year 2020 using ALS reference data. Only the spatially held-out regions were used. he dashed line indicates the 1:1 relationship and the red line shows the linear regression fit. The color scale indicates the number of observations per hexagonal bin and is shared across all panels

Table A2: Pooled absolute RMSE by canopy height bin for the four canopy height models. RMSE is reported in metres.

Height bin [m]	GEDI-Composite	GEDI-Spline	pDSM-Composite	pDSM-Spline
0–2	7.467	6.520	2.242	1.728
2–4	9.588	8.579	3.543	2.681
4–6	9.227	8.320	4.107	2.927
6–8	9.013	8.020	4.612	3.142
8–10	8.791	7.722	4.910	3.310
10–12	8.402	7.359	5.019	3.414
12–14	7.725	6.781	4.912	3.366
14–16	6.782	6.059	4.561	3.167
16–18	5.923	5.376	4.189	3.004
18–20	5.215	4.800	3.897	2.937
20–22	4.600	4.263	3.629	2.918
22–24	4.143	3.846	3.483	2.927
24–26	3.928	3.629	3.469	2.987
26–28	3.963	3.620	3.520	3.043
28–30	4.319	3.868	3.694	3.167
30–32	4.934	4.411	4.012	3.402
32–34	5.655	5.104	4.444	3.703
34–36	6.433	5.909	5.070	4.134
36–38	7.318	6.880	5.908	4.738
38–40	8.461	7.972	6.959	5.489

Table A3: Pooled relative RMSE by canopy height bin for the four canopy height models. Relative RMSE is reported as percentage relative to the reference canopy height.

Height bin [m]	GEDI-Composite	GEDI-Spline	pDSM-Composite	pDSM-Spline
0–2	899.8	785.7	270.2	208.2
2–4	318.9	285.4	117.9	89.2
4–6	183.4	165.4	81.6	58.2
6–8	128.3	114.2	65.7	44.7
8–10	97.5	85.6	54.4	36.7
10–12	76.2	66.7	45.5	31.0
12–14	59.2	52.0	37.7	25.8
14–16	45.1	40.2	30.3	21.0
16–18	34.8	31.6	24.6	17.6
18–20	27.4	25.2	20.5	15.4
20–22	21.9	20.3	17.3	13.9
22–24	18.0	16.7	15.2	12.7
24–26	15.7	14.5	13.9	12.0
26–28	14.7	13.4	13.0	11.3
28–30	14.9	13.4	12.8	10.9
30–32	15.9	14.3	13.0	11.0
32–34	17.2	15.5	13.5	11.2
34–36	18.4	16.9	14.5	11.8
36–38	19.8	18.7	16.0	12.9
38–40	21.8	20.5	17.9	14.1

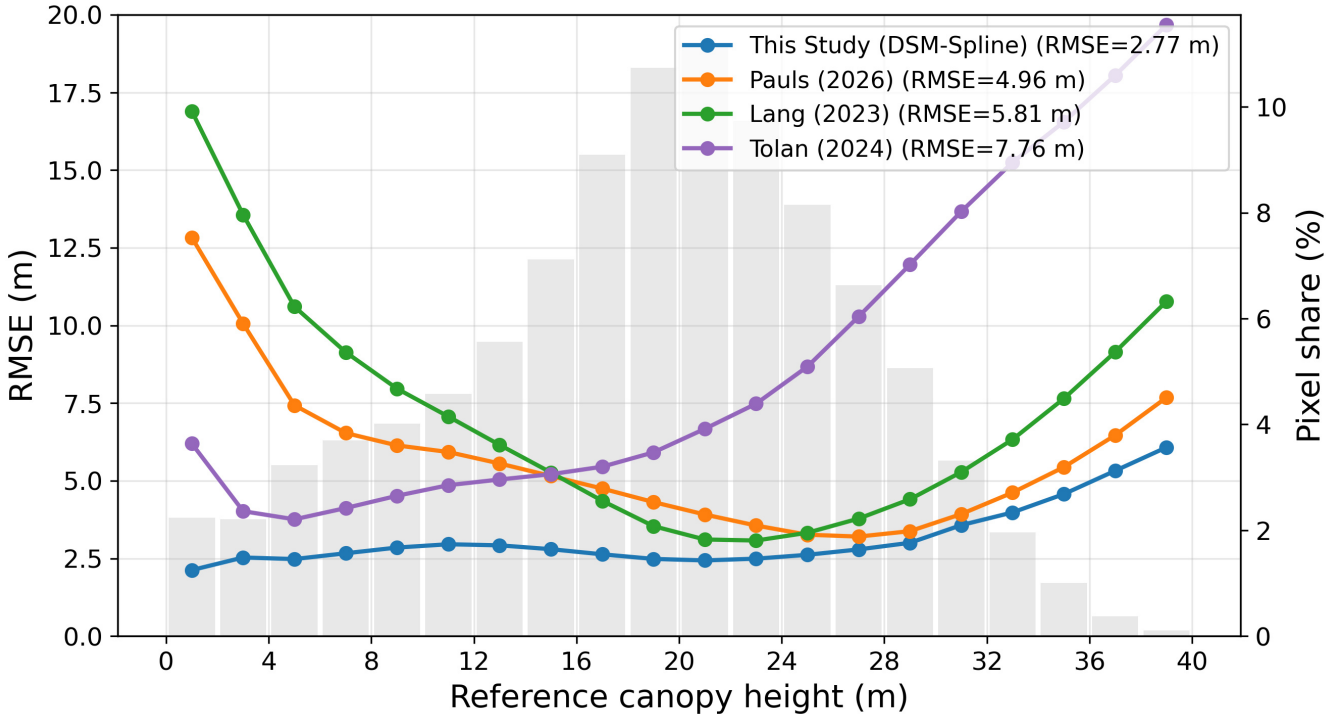


Figure A4: RMSE distribution comparison for the pDSM-Spline, Pauls 2026, Tolan 2024 and Lang 2023 canopy height models. Grey Bars correspond to the overall proportion of validation pixels within each bin.

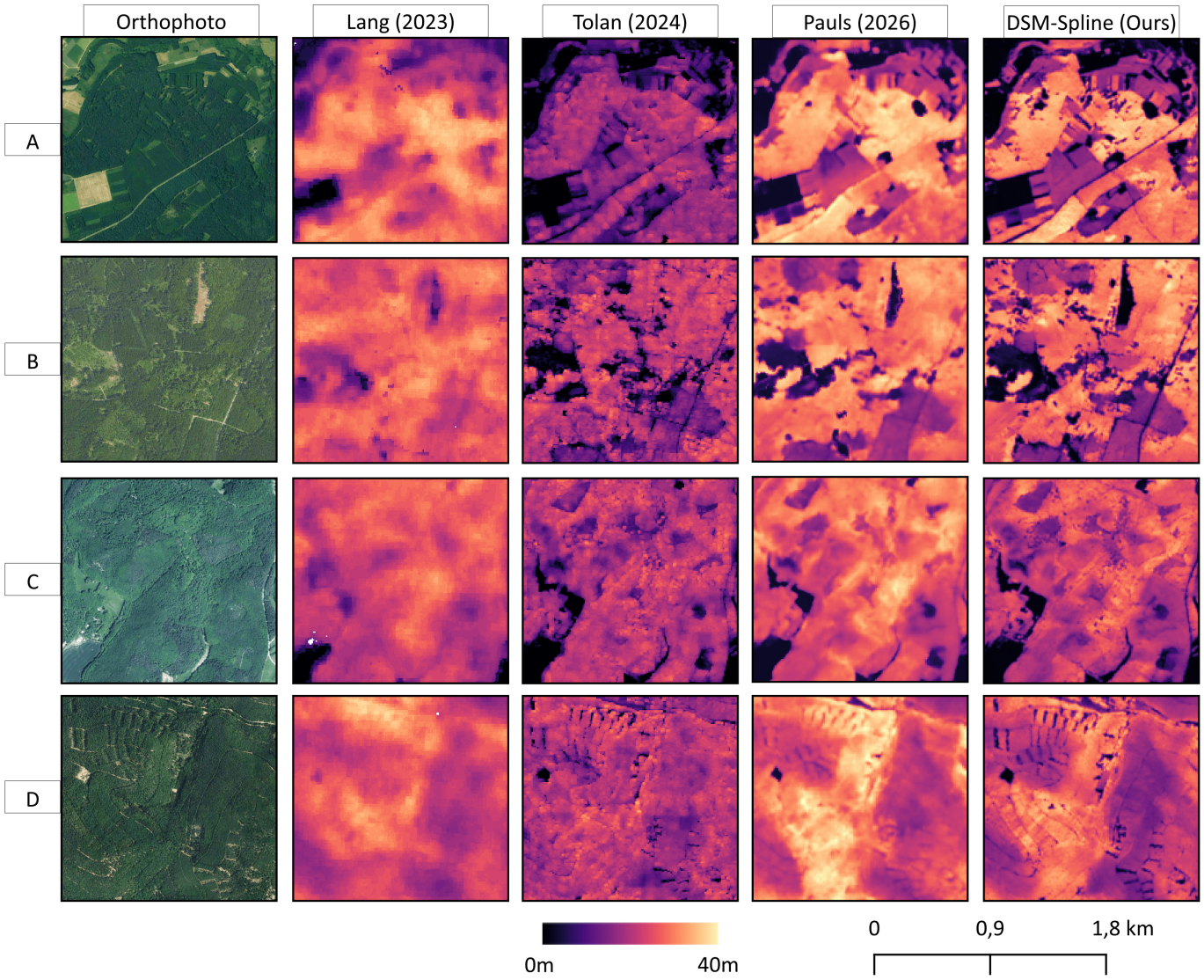


Figure A5: Visual comparison of different global canopy height maps and our pDSM-Spline model. The left row shows 2020 and 2021 orthophotos for context.